

1 Aqueous phase oligomerization of methyl vinyl 2 ketone through photooxidation 3 Part 1: Aging processes of oligomers

4 Pascal Renard¹, Frank Siekmann¹, Guillaume Salque², Carine Demelas¹, Bruno Coulomb¹,
5 Laurent Vassalo¹, Sylvain Ravier¹, Brice Temime-Roussel¹, Didier Voisin², Anne Monod¹

6
7 ¹ Aix-Marseille Université, CNRS, LCE FRE 3416, 13331, Marseille, France

8 ² Université Joseph Fourier, Grenoble 1 / CNRS-INSU, Laboratoire de Glaciologie et
9 Géophysique de l'Environnement, 54 rue Molière, 38402 Saint-Martin-d'Hères, France

10

11 Abstract

12 It has recently been established that unsaturated water soluble organic compounds (UWSOC)
13 might efficiently form oligomers in polluted fogs and wet aerosol particles, even for weakly
14 soluble ones like methyl vinyl ketone (MVK). The atmospheric relevance of these processes
15 is explored by means of multiphase process model studies in a companion paper. In the
16 present study, we investigate the aging of these aqueous phase MVK-oligomers formed *via*
17 $\cdot\text{OH}$ -oxidation, as well as their ability to form secondary organic aerosol (SOA) upon water
18 evaporation. The comparison between aqueous phase composition and aerosol composition
19 after nebulization of the corresponding solutions shows similar trends for oligomer formation
20 and aging. The measurements reveal that oligomer aging leads to the formation of organic
21 diacids. Quantification of the SOA mass formed after nebulization is performed, and the
22 obtained SOA mass yields seem to depend on the spectral irradiance of the light used to
23 initiate the photochemistry. Investigating a large range of initial MVK concentrations (0.2 –
24 20 mM), the results show that its $\cdot\text{OH}$ -oxidation undergoes competition between
25 functionalization and oligomerization that is dependent on the precursor concentration. At
26 high initial MVK concentrations ($\geq 2\text{mM}$), oligomerization prevails over functionalization,
27 while at lower initial concentrations, oligomerization is not the major process, and
28 functionalization dominates, resulting in small carbonyls, dicarbonyls and monoacids. The
29 atmospheric implications of these processes are discussed.

1 **1. Introduction**

2 Organic aerosol plays an important role in many atmospheric processes and has an important
3 impact on climate and human health. Globally, about 20 % of the organic aerosol mass is
4 emitted directly (Kanakidou et al., 2005; Spracklen et al., 2011), which conversely indicates
5 the relevance of aerosol formed by transformation of organic gas phase species, *i.e.* secondary
6 organic aerosol (SOA). The most commonly studied mechanism of SOA formation is the
7 oxidation of volatile organic compounds (VOC), which can lead to the formation of less
8 volatile species that subsequently partition into the condensed phase (Donahue et al., 2011;
9 Kanakidou et al., 2005; Kroll and Seinfeld, 2008; Hallquist et al., 2009). Nevertheless, the
10 oxidation of VOCs also results in more water soluble products that readily partition into the
11 aqueous phase (Blando and Turpin, 2000; Ervens et al., 2011; Epstein et al., 2013). Due to
12 further reactivity in the liquid phase, higher molecular weight and less volatile compounds
13 can be formed, which can remain at least in part in the condensed phase upon water
14 evaporation, thus leading to additional secondary organic aerosol formation through aqueous
15 phase reactions (aqSOA) (El Haddad et al., 2009; Carlton et al., 2009; Ervens et al., 2011;
16 Ortiz-Montalvo et al., 2012). In particular, Lee et al. (2012) observed a significant
17 enhancement of organic mass during the initial stage of oxidation of cloud water organics,
18 that they explained by functionalizing dissolved volatile organics *via* hydroxyl radical ($\cdot\text{OH}$)
19 oxidation. Aqueous phase processes can be very different from those in the gas phase, thus
20 leading to aqSOA with likely very different physical and chemical properties (Ervens et al.,
21 2011; Ortiz-Montalvo et al., 2012). These differences can explain that the oxidation state of
22 SOA formed during dry smog chamber experiments is significantly lower than that of ambient
23 SOA (Kroll and Seinfeld, 2008; Aiken et al., 2008; De Carlo et al., 2008; Ng et al., 2010; Lee
24 et al., 2012).

25 Volkamer et al. (2007) suggested that chemical processes in the aqueous phase of hygroscopic
26 particles, such as wet aerosol, can efficiently contribute to aqSOA mass. Besides, wet aerosol
27 provides higher precursor concentrations than in cloud and fog water droplets and reside in
28 the atmosphere over hours or days (Ervens et al., 2011), suggesting a significant role for
29 aqSOA formation in wet aerosol, in particular, in regions with high relative humidity (Carlton
30 and Turpin, 2013) and hygroscopic aerosol. Isoprene has the largest global atmospheric
31 emissions, estimated at $\sim 600 \text{ Tg yr}^{-1}$ of all non-methane VOCs (Guenther et al., 2006). Its key
32 oxidation products, *i.e.* methacrolein (MACR) and hydroperoxides (Kroll et al., 2006) are
33 known to contribute directly to the formation of SOA in the atmosphere. Methyl vinyl ketone

1 (MVK) is the other main gas-phase oxidation product of isoprene, yielding from 32 to 44 %
2 (Lee et al., 2005, Kroll et al., 2006). Unlike MACR, MVK does not lead to the formation of
3 SOA during its gas phase photooxidation (Kroll et al., 2006; Surratt et al., 2006), likely
4 because of the lack of an aldehydic hydrogen which precludes the formation of acidic
5 products such as 2,3-dihydroxymethacrylic acid (2-MGA) for further particle-phase
6 esterification reactions (Surratt et al., 2006). However, these results were obtained in smog
7 chamber experiments performed under dry conditions where aqueous phase processes were
8 excluded.

9 The photooxidation of carbonyl compounds has been studied in the aqueous phase, and their
10 ability to form oligomers and potentially aqSOA was shown (Altieri et al., 2006 and 2008;
11 Carlton et al., 2006 and 2007; Perri et al., 2009; El Haddad et al., 2009; Tan et al., 2009, 2010
12 and 2012; Zhang et al., 2010; Zhao et al., 2012; Liu et al., 2012; Ortiz-Montalvo et al., 2012;
13 Lim et al., 2013; Renard et al., 2013; Kameel et al., 2013; Kameel et al., 2014; Daumit et al.,
14 2014). In particular, Renard et al. (2013) showed that $\cdot\text{OH}$ oxidation of MVK in the aqueous
15 phase proceeds via a radical mechanism leading to oligomers which molecular masses up to
16 1800 Da, with the precursor initial concentration from 2 to 20 mM. At lower precursor initial
17 concentrations (e.g. 0.2 mM of MVK), Renard et al. (2013) observed lower weight molecular
18 compounds (up to m/z 300), and Zhang et al. (2010) observed the formation of small oxidized
19 compounds, such as methylglyoxal, formaldehyde, acetic, formic and pyruvic acids; thus
20 suggesting a competition between functionalization and oligomerization at these low initial
21 concentrations.

22 Liu et al. (2012) showed the ability of the generated oligomers to form SOA after water
23 evaporation. It is thus likely that the atmospheric impact of MVK reactivity, and especially its
24 ability to form SOA, is very different under dry and humid conditions.

25 The aim of the present study is to investigate the aging of the oligomers formed through
26 aqueous phase photooxidation of MVK. We determine the SOA chemical composition during
27 the formation and aging of the aqueous phase oligomers and we revisit the corresponding
28 SOA mass yields. A large range of initial precursor concentrations (from 0.2 to 20 mM) is
29 investigated in order to study the competition between functionalization and oligomerization.

30

1 **2. Experimental**

2 A photoreactor was used to simulate the aqueous phase photooxidation of MVK. $\cdot\text{OH}$
3 radicals were generated from H_2O_2 photolysis (Table 1). The liquid phase was analyzed using
4 a variety of analyzers for qualitative and quantitative characterization of the solution (detailed
5 in section 2.2).

6 For aerosol generation, aliquots of the solution were sampled from the photoreactor at specific
7 reaction times, then nebulized and dried prior to aerosol characterization using a scanning
8 mobility particle sizer (SMPS) and a high resolution time-of-flight aerosol mass spectrometer
9 (AMS) (Figure 1). Each experiment, i.e. aqueous phase photooxidation and aerosol
10 generation, was repeated at least once.

11 **2.1 Photoreactor**

12 The photoreactor set-up was based on the one described by Renard et al. (2013). It was a 450
13 cm^3 Pyrex thermostated photoreactor, equipped with a 1000 Watt Xenon arc lamp (LOT-
14 Oriel, LSH 601) and a glass filter (ASTM 490 AM 0). The resulting spectral irradiance into
15 the reactor is compared to that of the sun at sea level for a 48.3° zenith angle in Figure S1
16 (Supplementary information 2). All experiments were performed at 25°C and started with
17 irradiation of UHQ water ($18.2\text{ M}\Omega\text{ cm}$, Millipore), then H_2O_2 (Acros, 30 %, non-stabilized)
18 was introduced, and after 10 min of H_2O_2 photolysis, MVK (Sigma Aldrich, 99 %) was
19 introduced at time 0.

20 Tan et al. (2010) and Renard et al. (2013) have shown the important impact of initial
21 concentrations on oligomer formation. The experiments were thus carried out with various
22 MVK initial concentrations (Table 1), i.e., 0.2, 0.5, 2, 5 and 20 mM, corresponding to 9.6 to
23 960 mgC L^{-1} . Considering MVK as a proxy for UWSOC, this concentration range is
24 comprised in the range of the estimated total UWSOC concentrations from fog droplets to wet
25 aerosol (Renard et al., 2013).

26 The 50 cm^3 gas phase head space of the photoreactor was opened to ambient air for a few
27 seconds during each sampling. We verified in control experiments that this procedure induced
28 insignificant losses of MVK from the solution. Since the photoreactor was closed most of the
29 time, this procedure also induced a decrease in the dissolved O_2 concentrations, at a rate that
30 was dependent on the initial reactant concentrations, as shown in the companion paper by
31 Ervens et al.

1 The initial H₂O₂ concentrations were chosen in order to obtain a ratio ($\frac{[H_2O_2]_0}{[MVK]_0} = 20$), in order
2 to favor \cdot OH reaction with MVK rather than with H₂O₂ by more than 90 %. Under these
3 conditions, \cdot OH concentrations were estimated in the range (2 - 6) $\times 10^{-14}$ M (see
4 supplementary information 3), which falls in the range of the estimated values for \cdot OH
5 concentrations in cloud and fog droplets (Herrmann et al., 2010; Ervens and Volkamer, 2010
6 and Arakaki et al., 2013).

7 **2.2 Aqueous phase characterization**

8 Aliquots of the solution sampled from the photoreactor were analyzed for qualitative structure
9 elucidation of the oligomers using ultra-performance liquid chromatography mass
10 spectrometry (UPLC-ESI-MS); and for quantitative studies of the concentrations of i) MVK
11 and H₂O₂ by liquid chromatography coupled to UV detection (UHPLC-UV), ii) carboxylic
12 acids by ion chromatography-mass spectrometry (IC-ESI-MS), and iii) oligomers using
13 preparative liquid chromatography associated to total organic carbon (TOC) analyses.

14 *2.2.1 UPLC-ESI-MS analyses*

15 Aliquots of the solution sampled from the photoreactor were analyzed for organic species
16 using an ultra-high performance liquid chromatographic system coupled to a time of flight
17 mass spectrometer equipped with an electrospray source and an ion mobility cell (Synapt-G2
18 HDMS, Waters). The mass spectrometer was tuned to V-mode with a resolving power of
19 18000 at m/z 400. The mass accuracy (< 5 ppm) allowed for the determination of elemental
20 composition of organic species (Renard et al., 2013 and 2014), using the I-FIT software. The
21 I-FIT isotope predictive filtering is a strategy to reduce the number of proposed elemental
22 compositions using algorithms to estimate the number of carbon, oxygen atoms in an
23 unknown molecule based on the mass of the molecular ion and the relative intensity of the
24 first two most abundant isotopes (Hobby, 2005).

25 All parameters used are detailed in Renard et al. (2013). Briefly, the chromatographic
26 separations were carried out on an UPLC column (Waters, HSS T3 C18, 2.1 * 100 mm – 1.8
27 μ m) at 40°C. The mobile phases consisted in (A) 0.1 % formic acid (Biosolve, 99 %) in water
28 and (B) acetonitrile (Biosolve, ULC/MS). The gradient elution was performed at a flow rate
29 of 600 μ L min⁻¹ using 5 to 95 % of B within 7 min and held at 95 % of B for 1.5 min. The
30 sample injection volume was 10 μ L.

31 During each chromatographic run, leucine enkephalin (Waters, 2 ng μ L⁻¹, C₂₈H₃₇N₅O₇) was
32 used for lock-mass correction to obtain accurate masses for each organic component eluting

1 from the column. Optimum ESI conditions were found using a 0.5 kV capillary voltage, 40 V
2 sample cone voltage, 450°C desolvation temperature, 120°C source temperature, 20 L h⁻¹
3 cone gas flow rate and 800 L h⁻¹ desolvation gas flow rate.

4 All products were detected as their protonated molecules ([M + H]⁺) or sodium adducts ([M +
5 Na]⁺) in the positive mode, and their deprotonated molecules ([M - H]⁻) in the negative
6 mode. Data were collected from *m/z* 50 to 1800 in both ionization modes.

7 2.2.2 UHPLC-UV analyses

8 An ultra-high performance liquid chromatographic (UHPLC) system (ThermoScientific,
9 Accela 600 auto sampler and Accela 600 pump) coupled to a diode array detector
10 (ThermoScientific, Accela 600 PDA detector) was used to monitor the concentrations of
11 MVK and H₂O₂ sampled from the photoreactor. The chromatographic separation was
12 performed using a column (ThermoScientific, Hypersil GOLD, 100 x 2.1 mm - 1.9 μm) at
13 40°C and a flow rate of 300 μL min⁻¹. The mobile phase was water/acetonitrile (98:2) (v/v)
14 and the injection volume was set to 2 μL. The spectra were recorded from 200 to 360 nm.

15 Under these conditions, H₂O₂ has a retention time of 0.5 minutes and is chromatographically
16 separated from MVK which has a retention time of 1.8 minutes. The UV spectrum of aqueous
17 H₂O₂ exponentially increases with decreasing wavelength, it becomes intense below 300 nm.
18 Aqueous solutions of MVK show an intense absorption band (K-band; π → π* transition) that
19 peaks at 211 nm and a weak absorption band (R-band; n → π* transition) that peaks at 308
20 nm. The chromatograms were monitored at 270, 229 nm and 211 nm and the peak areas were
21 found to be directly proportional to both the H₂O₂ and the MVK concentrations in the range
22 of the studied concentrations: at 211 nm for low MVK concentrations ([MVK] ≤ 0.5 mM), at
23 229 nm for 2 ≤ [MVK] ≤ 20 mM), and at 270 nm for H₂O₂ concentrations.

24 2.2.3 IC-ESI-MS analyses

25 Quantification of organic acids in the solutions was performed with an ion chromatography
26 system (Dionex ICS3000) driven by Chromeleon[®] software (6.80 version), composed of a
27 gradient pump (Dionex SP-5), an autosampler (Dionex AS40), a conductivity detector
28 (Dionex, CD25) and coupled to a quadrupole mass spectrometer (Thermo Scientific Surveyor
29 MSQ) operated in the negative electrospray ionization (ESI) mode, using nitrogen gas flow of
30 6 L h⁻¹, 40 psi, temperature 500°C; capillary voltage 3,5 kV; sample cone voltage 75 V. An
31 electrolytic suppressor (Dionex, 4 mm ASRS 300) operated in external water mode (7 mL
32 min⁻¹) was placed before the conductivity cell. An additional peristaltic pump was used during

1 measurements to wash the entrance cone of the mass spectrometer with water at a flow rate of
2 0.4 mL min⁻¹. The chromatographic separations were carried out on a column (Dionex,
3 IonPac AS11-HC, 4 x 250 mm) coupled to a guard column (Dionex, AG11-HC, 4 x 50 mm).
4 A 25 µL sample was injected automatically using a 25 µL loop injection valve. The analysis
5 was performed at 35°C, with a flow rate set at 0.8 mL min⁻¹. Eluent A (Ultra High Quality
6 water) and eluent B (100 mM NaOH) were flushed with purified helium gas for 30 min and
7 kept under nitrogen atmosphere during the procedure. Separation was carried out using the
8 following gradient (min, B %): 0, 1 %; 12, 5 %; 30, 19 %; 40, 40 %, 50, 1 %. The analytes
9 were monitored using the selected ion-monitoring (SIM) mode, and signal areas (counts min⁻¹)
10 of each peak were used for quantification.

11 2.2.4 TOC analyses

12 TOC measurements were associated to preparative liquid chromatography to separate the
13 oligomers from the small and/or volatile reactants and reaction products in the liquid samples,
14 in order to measure the oligomer mass yields in experiment A (see section 3.2.3). A total
15 organic carbon / total nitrogen (TOC/TN) analyzer (Analytik Jena, N/C2100S) with the non-
16 purgeable organic carbon (NPOC) method was used to quantify the produced oligomers in our
17 liquid samples.

18 The NPOC method consists in pre-purging samples with oxygen and pre-acidifying (at pH=2
19 with HCl) to remove the inorganic carbon and purgeable organic carbon. TOC is measured by
20 injecting the sample into a heated combustion tube (800°C) with an oxidation catalyst. The
21 CO₂ produced is measured by a non-dispersive infrared (NDIR) gas analyzer. TN is measured
22 in parallel using chemiluminescence detection (CLD).

23 2.3 Particle generation and characterization

24 For aerosol generation, 35 mL of the solution was sampled at specific reaction times (Table
25 1), and nebulized using an atomizer (TSI, 3079) with a flow rate of 3.5 L min⁻¹ (Figure 1).
26 The generated droplet flow was led through a silica gel diffusion dryer and diluted with
27 filtered ambient air (at 5 L min⁻¹, using a HEPA capsule filter). A small fraction of the sample
28 (≈ 0.4 L min⁻¹) was passed through a Nafion dryer (Permapure, MD-110), before entering a
29 small 100 mL glass mixing chamber and the on-line analytical devices. The obtained relative
30 humidity was constant during all experiments at ca. 15 % measured at the entrance of the
31 AMS (Figure 1). The nebulization time for each sample was 30 min and, to ensure constant
32 and reproducible aerosol generation, only the last 15 min of nebulization were employed for

1 data analysis. To avoid memory effects, before each nebulization experiment, the system was
2 flushed by nebulizing UHQ water for 30 min.

3 The number size distribution was measured using a scanning mobility particle sizer (SMPS),
4 (Grimm, SMPS+C) consisting of a differential mobility analyzer (L-DMA) with a
5 condensation particle counter (Grimm, CPC, 5.403). The analyzed particle size ranged from
6 11 to 1083 nm (scanned within 6 min and 43 s).

7 A high resolution time-of-flight aerosol mass spectrometer was used to measure the bulk
8 chemical composition of the non-refractory submicron particulate matter (De Carlo et al.,
9 2006; Canagaratna et al., 2007). The instrument was used under standard conditions
10 (vaporizer at 600°C and electron ionization at 70 eV), in the high sensitivity V-mode with a
11 resolving power of 2000 at m/z 200. Each measurement point was averaged for 2 min and 40 s
12 (MS- and PToF-cycle, 40 s each, 2 cycles per run). Mass spectra of filtered air, using a HEPA
13 capsule filter, were taken prior each series of nebulizing experiments in order to adjust the
14 m/z 44 entry of the fragmentation table due to gas phase CO₂.

15 The standard fragmentation table with the corrected air fragment column for our carrier gas
16 and the default values of relative ionization efficiency were used in the AMS data analysis
17 (Squirrel 1.51H and the software PIKA 1.10H).

18 **3. Results**

19 **3.1 Evidence for oligomer formation and aging**

20 During MVK-[•]OH oxidation, the aqueous phase composition was monitored and compared to
21 the composition of the corresponding nebulized solutions.

22 *3.1.1 Aqueous phase analyses*

23 For each experiment, the solution was directly monitored using UPLC-ESI-MS and UHPLC-
24 UV for reaction times up to 150 min (Table 1). This time was higher than the complete
25 consumption of MVK in order to study the formation of oligomers and their aging processes,
26 as illustrated in Figure 2.

27 During experiment B (*i.e.* [MVK]₀ = 5mM), after 5 minutes of reaction, no significant
28 formation of high molecular weight compounds (HMWC) was observed (Figure 2b), whereas
29 after 10 minutes of reaction, mass spectra show that oligomer systems were formed on the
30 whole range of the investigated m/z (50-1800), with a regular pattern of 70.042 amu, which
31 corresponds to the exact mass of MVK. At 50 minutes of reaction, the maximum of

1 oligomerization was reached (Figure 2c). At this time, we observed several series of MVK-
2 oligomers, corresponding to several initiator radicals identified by Renard et al. (2013) under
3 similar conditions. As an example, a tentative molecular structure of the most intense series is
4 given in Figure 2c and is highlighted in red in the mass spectrum. At that time, 90 % of MVK
5 was consumed. Finally, the intensities of all the oligomer series decreased simultaneously for
6 all masses with no change in the oligomer pattern up to 90 minutes. From this reaction time,
7 the mass spectra show a collapse of the regular pattern in both negative (Figure 2d, 150 min)
8 and positive modes, possibly corresponding to a drastic aging process in which oligomers
9 formed smaller molecules. This hypothesis is confirmed by a more global approach, using the
10 SMPS and the AMS analysis of the SOA formed after nebulization of the solutions.

11 3.1.2 *Aerosol composition of SOA generated after nebulization of the solutions*

12 Under similar conditions, we verified as done in a previous study (Liu et al., 2012) that
13 nebulization of the reacted solutions and subsequent aerosol particle drying processes induced
14 negligible chemical transformations of the oligomers compared to the aqueous phase
15 composition. It was thus meaningful to compare the compositions of aqueous phase and SOA
16 after nebulization.

17 The AMS mass spectra (Figure 3) show two dominant fragments, at m/z 43 and m/z 44,
18 corresponding to $C_2H_3O^+$ and CO_2^+ fragments respectively. The time profiles of the AMS
19 total organic mass and both fragments clearly show (Figure 3) a similar kinetic behavior as
20 the one described above in section 3.1.1 for the corresponding solutions (Figure 2). Until 10
21 min of reaction, the intensity of the AMS total mass remains low (Figure 3a) and the mass
22 spectrum at 5 min (Figure 3b) is not significantly different from the one obtained by
23 nebulizing an aqueous solution containing the reactants before reaction, with m/z fragments
24 lower than 100. Then, the total mass increases to reach a maximum at 50 min (Figure 3c), an
25 order of magnitude higher than at 5 min. The mass spectrum is dominated by the m/z 43
26 fragment (Figure 3c). This observation is likely due to fragmentation by electronic impact of
27 oligomers containing repetitive carbonyl functions such as those identified in the aqueous
28 phase as shown by the example of a tentative molecular structure in Figure 2c. Finally, the
29 intensity of both the total organic mass and that of m/z 43 fragment decrease, the one of m/z
30 44 increases, and they both dominate the AMS mass spectrum with the same intensity at the
31 end of our investigation (150 min, Figure 3d).

32 Furthermore, comparing the AMS mass spectra between 50 and 150 min at higher masses
33 (m/z 100 – 200) (Figure 4), it is clear that at 50 min of reaction, the mass spectrum contains

1 more fragments in this range, than at 150 min. It is thus likely that the oligomers are being
2 significantly photooxidized through a fragmentation mechanism that forms smaller acidic
3 compounds, as observed by Aljawhary et al. (2013) for different precursors, and it confirms
4 the oligomer aging process suggested in Figure 2. After 50 min, oligomer fragmentation
5 prevails over oligomer formation.

6 For the quantitative study (see section 3.2), we used the data provided by the SMPS analysis.
7 Note that the overall collection efficiencies (CE) of the AMS in our experiments varied from
8 0.07 to 0.21, related to the SMPS signal. These low CE values, compared to chamber studies
9 or ambient aerosols, can be due to particle bounce at the vaporizer surface before
10 volatilization and to the shape and size-dependent transmission of the aerodynamic lens. As a
11 result, the studied compounds did not volatilize sufficiently fast at standard AMS vaporizer
12 temperatures to be fully detected (Liu et al., 2007; Docherty et al., 2013; Miyakawa et al.,
13 2013). In addition to these effects, it is possible that our low CE values were also due to the
14 particle size range (50 nm - 150 nm mass distribution), as the lowest part of this size range
15 corresponds to the region where the AMS transmission curve varies greatly (Liu et al., 2007).
16 This effect is confirmed by the fact that our lowest values for CE (0.07) were obtained for the
17 lowest MVK initial concentrations (0.2 – 2 mM) where the smallest particles were formed (50
18 nm mass distribution).

19 **3.2 Quantitative study of SOA**

20 *3.2.1 SOA mass*

21 For experiment B, Figure 5a shows a continuously increasing number size distribution with
22 reaction time from 5 to 150 min, with an increasing mode size during the two first kinetic
23 steps (up to 50 min), and a decreasing mode size during the third one, which corresponds to
24 oligomer aging. In order to determine the particle mass concentrations, we used the method
25 described by Kuwata et al. (2012) (eq. 1) to determine the density (ρ_{org}) of the SOA generated
26 in our system at each reaction time t ,

27

$$28 \quad \rho_{org, t} \text{ (g cm}^{-3}\text{)} = \frac{12+1 \times (\text{H/C})_t + 16 \times (\text{O/C})_t}{7+5 \times (\text{H/C})_t + 4.15 \times (\text{O/C})_t} \quad (\text{eq. 1})$$

29

30 where $(\text{O/C})_t$ and $(\text{H/C})_t$ are elemental ratios at reaction time t , as determined by the AMS
31 analysis of the SOA formed in our system. These ratios extend to the same ranges as those

1 used by Kuwata et al. (2012), and the resulting particle densities are reported in Table 2 and
2 Table 3. In particular, Table 2 shows a substantial change in the H/C (decrease) and O/C
3 (increase) after 50 min of reaction, t_{max} , for which the maximum SOA mass is reached,
4 denoting the oligomer aging and inducing an increase of the aerosol density.
5 Using these particle densities, the total mass concentrations were determined, and the time
6 evolution of the resulting distribution particle mass concentrations is shown in Figure 5b for
7 experiment B. The blank signal was determined prior to each individual experiment by
8 nebulizing pure water samples and was subtracted in the results for the mass calculation. At
9 the initial reaction time (0 min), the particle size distribution was determined by nebulizing an
10 aqueous mixture of the reactants (using experiment B concentrations), it showed a mass
11 concentration ($11.0 \pm 1.4 \mu\text{g m}^{-3}$) not statistically different from the one obtained by
12 nebulizing pure water, assuming a density of 1.1 g cm^{-3} . This confirms that the reactants are
13 too volatile to form substantial amounts of organic aerosol by nebulization of the solution
14 prior to reaction.
15 Confirming the UPLC-ESI-MS aqueous phase analyses (see section 3.1.1) and the AMS
16 results (see section 3.1.2), a similar kinetic behavior is also observed on the SMPS total mass
17 concentrations (Figure 5b and Figure 6). A slow increase is observed during the first step (0 –
18 10 min). Then oligomerization takes place corresponding to a fast increase of the SMPS mass,
19 until 50 min. Finally, after this maximum of oligomerization, a significant decrease of the
20 SMPS mass is observed. This decrease may be related to the decrease in the particle size
21 (Figure 5a), which can be due to the decrease of the oligomer size, by fragmentation of the
22 oligomers. It is thus likely that the oligomer aging forms more volatile compounds that the
23 SMPS does not measure. The high correlation between the total aerosol mass concentration
24 and the consumed MVK observed in Figure 6 from 0 to 50 min, allows for the determination
25 of the SOA mass yield, as discussed in section 3.2.3.

26 3.2.2 *Influence of initial MVK concentrations*

27 The influence of the initial aqueous phase concentration of MVK on the SOA formation was
28 investigated over a wide range, *i.e.* from 0.2 to 20 mM (Table 1). Not surprisingly, Figure 7
29 shows that the total aerosol mass concentration increases with increasing initial MVK
30 concentration. This observation is in very good agreement with the influence of MVK initial
31 concentration on the oligomerization process observed in the aqueous phase by Renard et al.
32 (2013). For experiments D and E, corresponding to the lowest initial MVK concentrations, the
33 SMPS and AMS signals were low, and they could be influenced by water impurities, whereas

1 no such influence was observed for experiments A, B and C. This is why the signal obtained
2 from the blank experiments was subtracted only for experiments D and E in Figure 7.
3 Moreover, Figure 7 clearly shows a different kinetic behavior of the SOA mass concentration
4 from the lowest initial concentration experiments (D and E), compared to the three highest
5 ones (experiments A, B and C). For experiments A, B and C, the SOA mass concentration
6 increases rapidly, reaches a maximum, and then decreases, while for experiments D and E, the
7 signal slowly increases and does not reach a maximum. This particular evolution may be due
8 to different chemical mechanisms occurring at different initial concentrations. We
9 hypothesized the predominance of oligomerization at 2 mM initial concentration and above,
10 this is further discussed in section 4.

11 The continuous increase of the particle number (shown in Figure 5a for experiment B) with
12 reaction time was observed for all initial concentrations (experiments A to E), whereas the
13 decrease of the size mode (in the number size distributions, after t_{max}) was observed for the
14 three highest initial concentrations only (experiments A, B and C) and not for experiments D
15 and E, *i.e.* only during oligomer aging.

16 3.2.3 SOA mass yields

17 The SOA mass yields, Y_t , were calculated at each reaction time step t from eq. 2.

$$18 \quad Y_t = \frac{[SOA]_t}{\Delta[MVK]_t} \quad (\text{eq. 2})$$

19 Where $\Delta[MVK]_t$ is the consumed [MVK] in mg L^{-1} at reaction time t ; and $[SOA]_t$ is the
20 formed SOA mass at reaction time t , in mg per L of evaporated water. This term takes into
21 account the SOA mass (M_{SMPS}) measured by the SMPS at time t (in $\mu\text{g m}^{-3}$), the atomizer flow
22 ($F_{atomizer}$ in L m^{-3}), the dilution (f_{dil}), and the transmission efficiency in our nebulizing system
23 (T_{eff} in %) (see Table S1).

$$24 \quad [SOA]_t = \frac{M_{SMPS} \times T_{eff}}{F_{atomizer} \times f_{dil} \times 1000} \quad (\text{eq. 3})$$

25 The yields obtained at t_{max} for experiments A, B and C are shown in Table 3. Although the
26 total SOA mass (at t_{max}) increases linearly with the initial concentration for these three
27 experiments, the yields are statistically identical as well as their H/C and O/C ratios. Due to
28 the very large uncertainties of our yield determinations (see below), it is not possible to use
29 these data (Table 2 and 3) to provide any interpretation on the possible effect of initial
30 concentrations on the yields. In contrast, the O/C and H/C ratios clearly show statistically
31 stable values when the total particle mass increases from 100 to 900 $\mu\text{g/m}^3$ (Table 3). It is thus

1 likely that the total mass loading does not influence the relative oxygenation of the SOA
2 produced (at t_{max}) under our experimental conditions.

3 Although the particle mass loadings (M_{SMPs}) were accurately measured, our yield
4 determinations were affected by large uncertainties due to the estimation of the transmission
5 efficiency in our nebulizing system (see supplementary information 1, Table S1). In order to
6 confirm these yields' values, another method was tested for experiment A at 90 min of
7 reaction (*i.e.* close to t_{max}). Preparative chromatography was performed using UPLC, where
8 small molecules were separated from the oligomers using a divert valve, at retention times
9 lower than 2 min. The solution containing oligomers was accumulated, concentrated and
10 analyzed using a TOC analyzer. From the carbon mass, we deduced the total mass using the
11 H/C and O/C ratios given by the AMS. The yield was then directly calculated from the total
12 mass of sample (in mg L^{-1}) divided by the mass of consumed MVK at the same reaction time.
13 A yield of 59 ± 5 % (in mass) was obtained with this method at 90 min of reaction, thus
14 statistically similar from the one obtained by the nebulizing method (70 ± 50 %) at t_{max} .

15 These yields are significantly higher than those obtained by Liu et al. (2012) who obtained
16 yields up to 9.9 % under similar experimental conditions as ours. It is important to note that
17 these values were obtained assuming all the particle densities were 1 g cm^{-3} in Liu et al.
18 (2012), and also the transmission efficiency of the nebulizing system was calibrated with
19 NaCl solutions. However, it is likely that succinic acid or ammonium nitrate are more
20 adequate for the calibration, and we show in the supplementary information 1 (Table S1) that
21 the transmission efficiency of NaCl solutions are significantly different from the two other
22 solutions. The nebulizing system was slightly different, with a teflon bag in Liu et al. (2012)
23 that could enable i) larger amounts of wall losses for organic particles as compared to the
24 system presented here; but ii) longer particle residence times, leaving more time for gas-
25 particle equilibrium than in our system. However, our control experiment using preparative
26 chromatography confirms the high yield value obtained here, independent on the nebulizing
27 system and its calibration. The different yields obtained here as compared to the study by Liu
28 et al. (2012) may be due to the different irradiation Xe lamp used: 300 W, with a pyrex filter,
29 in Liu et al. (2012), and 1000 W, with a ASTM 490 AM 0 filter, in the present study. The
30 influence of the lamp spectra on SOA mass yields of other systems, *i.e.* gas phase
31 photooxidation of biogenic and anthropogenic precursors, have been previously observed in
32 atmospheric simulation chambers (Bregonzio-Rozier et al., 2014). We verified, using a
33 spectroradiometer (SR-501, LOT-Oriel), that the spectral irradiance of the 300W and the

1 1000W Xe lamps at $\lambda \geq 400$ nm represent respectively half and twice the solar irradiance
2 intensity at sea level, for a 48.3° zenith angle (Supplementary information 2, Figure S1). Due
3 to the high variability of the irradiance in the atmosphere at $\lambda \geq 400$ nm, as shown by the
4 Tropospheric Ultraviolet and Visible Radiation Model ([http://cprm.acd.ucar.edu](http://cprm.acd.ucar.edu/Models/TUV/Interactive_TUV/)
5 [/Models/TUV/Interactive_TUV/](http://cprm.acd.ucar.edu/Models/TUV/Interactive_TUV/)), both lamps can be seen as representative of the natural
6 irradiance in this wavelength range. However at 300 nm, the spectral irradiance of the 1000W
7 Xe lamp is 7 and 9 times higher than that of the direct solar irradiance (for a 48.3° zenith
8 angle) and the 300W Xe lamp respectively (Supplementary information 2, Figure S1). This
9 part of the spectrum is essential for photochemistry, and may induce different photochemical
10 processes: we verified that we observed the same series of oligomers as in Liu et al. (2012),
11 but with different relative intensities. The different spectral irradiance of the lights used at 300
12 nm may be the reason for the different yields obtained, but it needs to be confirmed by a
13 thorough study of the influence of the spectral irradiance in the UV, on the oligomer mass
14 yields.

15 It is interesting to note that the yields and densities obtained in the present study are in the
16 same range as those of a similar study with a different precursor, *i.e.* glycolaldehyde and a
17 different irradiation system even more intense in the UV, *i.e.* a 254-nm mercury lamp (Ortiz-
18 Montalvo et al., 2012). They reported aqSOA yields for oxidation products of glycolaldehyde
19 (1 mM) which decrease gradually with reaction time from about 120% to 50%; while the
20 calculated densities increase from 1.3 to 1.6 g cm⁻³.

21 **4. Discussion**

22 This section discusses the results obtained on the aging of the reaction products of MVK-[•]OH
23 experiments and the related oxidation processes in two ways. First, the competition between
24 functionalization and oligomerization and the subsequent aging according to the initial
25 concentration of MVK is discussed; and second, a Van Krevelen diagram, *i.e.*, H/C vs O/C
26 ratios) of the obtained SOA is presented and compared to previous studies.

27 **4.1 MVK functionalization versus oligomerization: influence of initial concentration**

28 In order to compare our work with the aging of organic aerosol in the atmosphere compiled
29 by Ng et al. (2010), we used the AMS data, and in particular, the two dominant fragments,
30 m/z 44 (CO₂⁺) and m/z 43 (C₂H₃O⁺), observed in our study. More precisely, we focused on the
31 ratio of m/z 44 and m/z 43 to total organic aerosol, f_{44} and f_{43} , respectively. In Ng et al. (2010),
32 low volatility oxygenated organic aerosol (LV-OOA) has higher f_{44} than semi-volatile

1 oxygenated organic aerosol (SV-OOA) which in turn has higher f_{43} values. Despite the very
2 different conditions, it is interesting to compare our aging data with those compiled from field
3 studies and other aqueous phase experiments. Figure 8 compares our f_{44} versus f_{43} values to
4 those provided in the compilation by Ng et al. (2010) as well as the nebulization data by Lee
5 et al. (2011a). It is clear from this figure that the SOA composition and its evolution highly
6 depend on the initial MVK concentration. For the three highest initial concentrations
7 (experiments A, B and C), oligomerization takes place with the formation of oligomers
8 containing repetitive carbonyl functions such as those identified in the aqueous phase (Figure
9 2c), inducing an important increase of f_{43} and a simultaneous decrease of f_{44} , roughly up to
10 t_{max} . After t_{max} , most of the initial MVK is consumed, slowing down the oligomerization
11 process, and an important decrease of f_{43} and a simultaneous increase of f_{44} is observed, likely
12 due to oligomer aging, as detailed in section 3.1. At lower initial MVK concentrations
13 (experiments D and E), oligomerization seems much less important and oxidation is the
14 dominant process, as evidenced by the continuous increase of f_{44} . It can thus be suggested
15 that, at these lower initial concentrations, functionalization dominates over oligomerization,
16 and the aerosol is mainly composed of low-volatility organic acid and not of MVK-oligomers.
17 This observation is strengthened by the comparison of our results with those of previous
18 studies. Zhang et al. (2010) performed aqueous phase $\cdot\text{OH}$ oxidation of MVK (0.2 mM initial
19 concentration), and observed the formation of functionalization products, *i.e.* formaldehyde,
20 glyoxal, methylglyoxal, pyruvic, oxalic, formic, acetic, and malonic acids. Furthermore, for
21 experiments D and E ($[\text{MVK}]_0 \leq 0.5$ mM), our f_{44} - f_{43} plots are similar to those obtained using
22 a similar set-up, starting from pinonic acid, glyoxal and glyoxylic acid at similar and higher
23 initial concentrations (Lee et al., 2011a and 2011b). In particular, starting at 3 mM of glyoxal,
24 Lee et al. (2011b) obtained similar f_{44} - f_{43} plots as our experiments performed at much lower
25 initial concentrations ($[\text{MVK}]_0 \leq 0.5$ mM), thus showing that the concentration is not the only
26 important parameter in oligomerization processes, but the chemical nature of the precursor is
27 also fundamental.

28 MVK oligomerization occurs *via* saturation of the vinyl group (Renard et al., 2013). The
29 resulting radical monomer is stabilized by the resonance effect with the adjacent carbonyl
30 group and this stabilization decreases the enthalpy of polymerization and hence facilitates the
31 oligomerization in the aqueous phase compared to other molecules (Odian, 2004).

32

1 4.2 Oligomer aging processes

2 The Van Krevelen diagram (Figure 9) shows a significant increase of O/C and a significant
3 decrease of H/C with reaction time after t_{max} . When oligomerization is the dominating
4 process, almost no changes are observed in the van Krevelen diagram: the H/C and O/C
5 values are confined in a restricted circle until t_{max} . The atomic ratios for H/C and O/C of MVK
6 and the oligomers, with a degree of polymerization of 5, identified by Renard et al. (2013) are
7 also reported in this diagram. MVK, oligomers and the nebulized solutions until t_{max} are
8 confined in a circle that highlights the similarity of their structures.

9 After that time, the values of O/C (H/C) increase (decrease) out of the circle, thus denoting an
10 oligomer aging process. Changes in functionality of organic aerosol are traced in this diagram
11 along a line, whose slope is -0.6. A very similar slope value (-0.5) was interpreted by Ng et al.
12 (2011) as a COOH group addition to the site of a C-C bond cleavage, thus suggesting that the
13 oligomer aging process proceeds *via* fragmentation. This is also suggested by the time
14 evolution of the particle number size distributions (Figure 5a: see section 3.2.1). While a
15 continuous increase of the particle number with reaction time was observed for all initial
16 concentrations, a significant decrease of the size mode was observed after t_{max} for the highest
17 concentrations only (experiments A, B and C), *i.e.* during oligomer aging. This size mode
18 decrease was also correlated with a decreasing total mass (Figure 5b). These observations, in
19 combination with the fact that f_{44} increases during oligomer aging, indicate that the oligomer
20 aging proceeds *via* fragmentation processes that generate smaller (or more volatile) and more
21 acidic compounds.

22 The formation of carboxylic acids in the aqueous phase was monitored during the course of
23 the reaction. In good agreement with Zhang et al. (2010), small volatile monocarboxylic acids
24 such as acetic, formic and pyruvic acids were formed as primary reaction products from MVK
25 reactivity. We further observed the formation of diacids as secondary or tertiary reaction
26 products, such as oxalic, malonic, succinic (Figure 10) malic and tartaric acids (not
27 quantified). Finally, the formation of these diacids started at t_{max} , and was correlated to the
28 increase of the AMS m/z 44 (CO_2^+) signal observed from the nebulized solutions. It is thus
29 likely that the oligomer aging proceeds *via* fragmentation (by $\cdot\text{OH}$ oxidation and/or
30 photolysis), leading to the formation of smaller partially oxidized products, *i.e.*, hydroxyacids
31 or ketoacids (such as those identified by Jaoui et al., 2006), which, in turn are oxidized into
32 stable diacids.

1 **5. Atmospheric implications**

2 Considering the results obtained here on oligomer formation and aging from MVK at varying
3 initial concentrations together with those obtained by previous studies on the identification of
4 the low-molecular-weight compounds products of the reaction (Zhang et al., 2010), a general
5 scheme of the potential atmospheric fate of MVK in the aqueous phase is shown on Figure 11.
6 MVK \cdot OH-oxidation undergoes kinetic competition between functionalization and
7 oligomerization, depending on the precursor initial concentration. At 2 mM of MVK and
8 above this concentration, oligomerization dominates over functionalization. At these
9 concentrations, \cdot OH-oxidation of MVK forms oligomers that are SV-OOA, with low O/C
10 (lower than 0.50) and high f_{43} . Oligomers are then fragmented, *via* unidentified intermediates
11 that have the properties of LV-OOA (with increasing O/C and decreasing H/C, Figure 9)
12 which then form organic diacids. For lower initial MVK concentrations (< 2 mM),
13 oligomerization is not the major process, and functionalization dominates, ending into small
14 carbonyls, dicarbonyls and acids that were identified by Zhang et al. (2010) (Figure 11).

15 Among the atmospherically relevant alkenoic alcohols, acids, ketones and aldehydes, *i.e.*,
16 UWSOC, although MVK is one of the most abundant species, it is one of the most volatile
17 ($P_{\text{sat}} = 10^{-5} - 0.1$ atm, with $P_{\text{sat(MVK)}} = 0.1$ atm at 25°C; Asher and Pankow 2006), and one of
18 the least soluble compounds ($K_{\text{H}} = 1 - 10^3$ M atm⁻¹, with $K_{\text{H(MVK)}} = 41$ M atm⁻¹ at 25°C; Iraci
19 et al., 1999). The atmospheric impacts of the processes shown here should thus be very
20 limited for MVK alone. However, the oligomerization mechanism undergone by MVK occurs
21 *via* saturation of the vinyl group (Renard et al., 2013), and the resulting radical monomer is
22 stabilized by the resonance effect with the adjacent carbonyl group thus decreasing the
23 enthalpy of polymerization facilitating the oligomerization in the aqueous phase compared to
24 other molecules. More generally, conjugation of the C=C with substituents such as the
25 benzene ring (styrene and *a*-methylstyrene), and alkene double bond (butadiene and isoprene),
26 the carbonyl linkage (acrylic acid, methyl acrylate, methyl methacrylate), and the nitrile group
27 (acrylonitrile) similarly leads to stabilization of the monomer and decreases enthalpies of
28 polymerization (O'dian, 2004). It is thus likely that a large number of atmospherically relevant
29 molecules can follow the same process either in the bulk or at the wet aerosol interface
30 (Kameel et al., 2013 and 2014). In this context, our results suggest that this class of
31 compounds can impact the aerosol composition, and contribute to aqSOA formation upon
32 water evaporation. The corresponding aqSOA mass yields seem to depend on the spectral
33 irradiance of the light used to initiate the photochemistry, but further studies are needed to

1 confirm this point. Finally, the aging of the oligomers formed could be an explanation, at least
2 in part, for the presence of diacids, such as oxalic, malonic and succinic acids, observed in the
3 ambient aerosol (Legrand et al., 2007; Kawamura et al., 2010). In Part 2 of this study, the
4 atmospheric relevance of these processes is explored by means of multiphase box model
5 studies.

6
7 *Acknowledgements.* We thank the National Research Agency ANR (project CUMULUS
8 ANR-2010-BLAN-617-01), AXA insurances, Région Rhone-Alpes (CIBLE program) and
9 CNRS-INSU (LEFE-CHAT AtmOrbitrap project) for funding this research. We also thank
10 Barbara Ervens (CIRES, University of Colorado, Boulder and Chemical Sciences Division,
11 National Oceanic and Atmospheric Administration (NOAA), Boulder, CO, USA) for valuable
12 scientific discussions on this topic; Etienne Quivet (Aix-Marseille university, Laboratory of
13 Chemistry of Environment) for proofreading and Assia Smaani (Aix-Marseille university,
14 Laboratory of Chemistry of Environment) for contributing to the experimental work on MVK
15 $\cdot\text{OH}$ -oxidation experiments.

16

1 **References**

- 2 Aiken, A. C., DeCarlo, P. F., Kroll, J. H., Worsnop, D. R., Huffman, J. A., Docherty, K. S.,
3 Ulbrich, I. M., Mohr, C., Kimmel, J. R., Sueper, D., Sun, Y., Zhang, Q., Trimborn, A.,
4 Northway, M., Ziemann, P. J., Canagaratna, M. R., Onasch, T. B., Alfarra, M. R., Prevot,
5 A. S. H., Dommen, J., Duplissy, J., Metzger, A., Baltensperger, U. and Jimenez, J. L.: O/C
6 and OM/OC Ratios of Primary, Secondary, and Ambient Organic Aerosols with High-
7 Resolution Time-of-Flight Aerosol Mass Spectrometry, *Environmental Science &*
8 *Technology*, 42(12), 4478–4485, doi:10.1021/es703009q, 2008.
- 9 Aljawhary, D., Lee, A. K. Y. and Abbatt, J. P. D.: High-resolution chemical ionization mass
10 spectrometry (ToF-CIMS): application to study SOA composition and processing,
11 *Atmospheric Measurement Techniques*, 6(11), 3211–3224, doi:10.5194/amt-6-3211-2013,
12 2013.
- 13 Altieri, K. E., Carlton, A. G., Lim, H.-J., Turpin, B. J. and Seitzinger, S. P.: Evidence for
14 Oligomer Formation in Clouds: Reactions of Isoprene Oxidation Products, *Environmental*
15 *Science & Technology*, 40(16), 4956–4960, doi:10.1021/es052170n, 2006.
- 16 Altieri, K. E., Seitzinger, S. P., Carlton, A. G., Turpin, B. J., Klein, G. C. and Marshall, A. G.:
17 Oligomers formed through in-cloud methylglyoxal reactions: Chemical composition,
18 properties, and mechanisms investigated by ultra-high resolution FT-ICR mass
19 spectrometry, *Atmospheric Environment*, 42(7), 1476–1490,
20 doi:10.1016/j.atmosenv.2007.11.015, 2008.
- 21 Arakaki, T., Anastasio, C., Kuroki, Y., Nakajima, H., Okada, K., Kotani, Y., Handa, D.,
22 Azechi, S., Kimura, T., Tshako, A. and Miyagi, Y.: A General Scavenging Rate Constant
23 for Reaction of Hydroxyl Radical with Organic Carbon in Atmospheric Waters,
24 *Environmental Science & Technology*, 130718140737000, doi:10.1021/es401927b, 2013.
- 25 Asher, W. E. and Pankow, J. F.: Vapor pressure prediction for alkenoic and aromatic organic
26 compounds by a UNIFAC-based group contribution method, *Atmospheric Environment*,
27 40(19), 3588–3600, doi:10.1016/j.atmosenv.2005.12.004, 2006.
- 28 Blando, J. D. and Turpin, B. J.: Secondary organic aerosol formation in cloud and fog
29 droplets: a literature evaluation of plausibility, 2000, 34(10), 1623–1632,
30 doi:10.1016/S1352-2310(99)00392-1, 2000.
- 31 Brégonzio-Rozier, L., Siekmann, F., Giorio, C., Pangui, E., Morales, S. B., Temime-Roussel,
32 B., Gratién, A., Michoud, V., Ravier, S., Tapparo, A., Monod, A. and Doussin, J.-F.:
33 Gaseous products and Secondary Organic Aerosol formation during long term oxidation of
34 isoprene and methacrolein, *Atmospheric Chemistry and Physics Discussions*, 14(16),
35 22507–22545, doi:10.5194/acpd-14-22507-2014, 2014.
- 36 Canagaratna, M. R., Jayne, J. T., Jimenez, J. L., Allan, J. D., Alfarra, M. R., Zhang, Q.,
37 Onasch, T. B., Drewnick, F., Coe, H., Middlebrook, A., Delia, A., Williams, L. R.,
38 Trimborn, A. M., Northway, M. J., DeCarlo, P. F., Kolb, C. E., Davidovits, P. and
39 Worsnop, D. R.: Chemical and microphysical characterization of ambient aerosols with the
40 aerodyne aerosol mass spectrometer, *Mass Spectrometry Reviews*, 26(2), 185–222,
41 doi:10.1002/mas.20115, 2007.
- 42 Carlton, A. G. and Turpin, B. J.: Particle partitioning potential of organic compounds is
43 highest in the Eastern US and driven by anthropogenic water, *Atmospheric Chemistry and*
44 *Physics*, 13(20), 10203–10214, doi:10.5194/acp-13-10203-2013, 2013.

- 1 Carlton, A. G., Turpin, B. J., Altieri, K. E., Seitzinger, S., Reff, A., Lim, H.-J. and Ervens, B.:
2 Atmospheric oxalic acid and SOA production from glyoxal: Results of aqueous
3 photooxidation experiments, *Atmospheric Environment*, 41(35), 7588–7602,
4 doi:10.1016/j.atmosenv.2007.05.035, 2007.
- 5 Carlton, A. G., Turpin, B. J., Lim, H.-J., Altieri, K. E. and Seitzinger, S.: Link between
6 isoprene and secondary organic aerosol (SOA): Pyruvic acid oxidation yields low volatility
7 organic acids in clouds, *Geophysical Research Letters*, 33(6), doi:10.1029/2005GL025374,
8 2006.
- 9 Carlton, A. G., Wiedinmyer, C. and Kroll, J. H.: A review of Secondary Organic Aerosol
10 (SOA) formation from isoprene, *Atmospheric Chemistry and Physics*, 9(14), 4987–5005,
11 2009.
- 12 Daumit, K. E., Carrasquillo, A. J., Hunter, J. F. and Kroll, J. H.: Laboratory studies of the
13 aqueous-phase oxidation of polyols: submicron particles vs. bulk aqueous solution,
14 *Atmospheric Chemistry and Physics*, 14(19), 10773–10784, doi:10.5194/acp-14-10773-
15 2014, 2014.
- 16 DeCarlo, P. F., Dunlea, E. J., Kimmel, J. R., Aiken, A. C., Sueper, D., Crouse, J., Wennberg,
17 P. O., Emmons, L., Shinozuka, Y., Clarke, A. and others: Fast airborne aerosol size and
18 chemistry measurements with the high resolution aerosol mass spectrometer during the
19 MILAGRO Campaign, *Atmos. Chem. Phys. Discuss*, 7(18), 269–18, 2007.
- 20 DeCarlo, P. F., Kimmel, J. R., Trimborn, A., Northway, M. J., Jayne, J. T., Aiken, A. C.,
21 Gonin, M., Fuhrer, K., Horvath, T., Docherty, K. S., Worsnop, D. R. and Jimenez, J. L.:
22 Field-Deployable, High-Resolution, Time-of-Flight Aerosol Mass Spectrometer,
23 *Analytical Chemistry*, 78(24), 8281–8289, doi:10.1021/ac061249n, 2006.
- 24 Docherty, K. S., Jaoui, M., Corse, E., Jimenez, J. L., Offenberg, J. H., Lewandowski, M. and
25 Kleindienst, T. E.: Collection Efficiency of the Aerosol Mass Spectrometer for Chamber-
26 Generated Secondary Organic Aerosols, *Aerosol Science and Technology*, 47(3), 294–309,
27 doi:10.1080/02786826.2012.752572, 2013.
- 28 Donahue, N. M., Epstein, S. A., Pandis, S. N. and Robinson, A. L.: A two-dimensional
29 volatility basis set: 1. organic-aerosol mixing thermodynamics, *Atmospheric Chemistry
30 and Physics*, 11(7), 3303–3318, doi:10.5194/acp-11-3303-2011, 2011.
- 31 Epstein, S. A., Tapavicza, E., Furche, F. and Nizkorodov, S. A.: Direct photolysis of carbonyl
32 compounds dissolved in cloud and fog~droplets, *Atmospheric Chemistry and Physics*,
33 13(18), 9461–9477, doi:10.5194/acp-13-9461-2013, 2013.
- 34 Ervens, B., Turpin, B. J. and Weber, R. J.: Secondary organic aerosol formation in cloud
35 droplets and aqueous particles (aqSOA): a review of laboratory, field and model studies,
36 *Atmospheric Chemistry and Physics*, 11(21), 11069–11102, doi:10.5194/acp-11-11069-
37 2011, 2011.
- 38 Ervens, B. and Volkamer, R.: Glyoxal processing by aerosol multiphase chemistry: towards a
39 kinetic modeling framework of secondary organic aerosol formation in aqueous particles,
40 *Atmospheric Chemistry and Physics*, 10(17), 8219–8244, doi:10.5194/acp-10-8219-2010,
41 2010.
- 42 Guenther, A., Karl, T., Harley, P., Wiedinmyer, C., Palmer, P. I., Geron, C. and others:
43 Estimates of global terrestrial isoprene emissions using MEGAN (Model of Emissions of
44 Gases and Aerosols from Nature), *Atmospheric Chemistry and Physics*, 6(11), 3181–3210,
45 2006.

- 1 Haddad, I. E., Liu, Y., Nieto-Gligorovski, L., Michaud, V., Temime-Roussel, B., Quivet, E.,
2 Marchand, N., Sellegri, K. and Monod, A.: In-cloud processes of methacrolein under
3 simulated conditions—Part 2: Formation of secondary organic aerosol, *Atmospheric*
4 *Chemistry and Physics*, 9(14), 5107–5117, 2009.
- 5 Hallquist, M., Wenger, J., Baltensperger, U., Rudich, Y., Simpson, D., Claeys, M., Dommen,
6 J., Donahue, N. M., George, C., Goldstein, A. H., Hamilton, J. V., Herrmann, H.,
7 Hoffmann, T., Iinuma, Y., Jang, M., Jenkin, M. E., Jimenez, J. L., Kiendler-Scharr, A.,
8 Maenhaut, W., McFiggans, G. B., Mentel, T. F., Monod, A., Prevot, A. S. H., Seinfeld, J.
9 H., Surratt, J. D., Szmigielski, R. and wild: The formation, properties and impact of
10 secondary organic aerosol: current and emerging issues, *Atmospheric Chemistry and*
11 *Physics*, 9(14), 5155–5236, doi:10.5194/acp-9-5155-2009, 2009.
- 12 Herrmann, H., Hoffmann, D., Schaefer, T., Brüner, P. and Tilgner, A.: Tropospheric
13 Aqueous-Phase Free-Radical Chemistry: Radical Sources, Spectra, Reaction Kinetics and
14 Prediction Tools, *ChemPhysChem*, 11(18), 3796–3822, doi:10.1002/cphc.201000533,
15 2010.
- 16 Hobby, K.: A novel method of isotope prediction applied to elemental composition analysis,
17 2005.
- 18 Iraci, L. T., Baker, B. M., Tyndall, G. S. and Orlando, J. J.: Measurements of the Henry's law
19 coefficients of 2-methyl-3-buten-2-ol, methacrolein, and methylvinyl ketone, *Journal of*
20 *atmospheric chemistry*, 33(3), 321–330, 1999.
- 21 Jaoui, M., Corse, E., Kleindienst, T. E., Offenberg, J. H., Lewandowski, M. and Edney, E. O.:
22 Analysis of Secondary Organic Aerosol Compounds from the Photooxidation of d -
23 Limonene in the Presence of NO X and their Detection in Ambient PM 2.5, *Environmental*
24 *Science & Technology*, 40(12), 3819–3828, doi:10.1021/es052566z, 2006.
- 25 Jimenez, J. L., Canagaratna, M. R., Donahue, N. M., Prevot, A. S. H., Zhang, Q., Kroll, J. H.,
26 DeCarlo, P. F., Allan, J. D., Coe, H., Ng, N. L., Aiken, A. C., Docherty, K. S., Ulbrich, I.
27 M., Grieshop, A. P., Robinson, A. L., Duplissy, J., Smith, J. D., Wilson, K. R., Lanz, V.
28 A., Hueglin, C., Sun, Y. L., Tian, J., Laaksonen, A., Raatikainen, T., Rautiainen, J.,
29 Vaattovaara, P., Ehn, M., Kulmala, M., Tomlinson, J. M., Collins, D. R., Cubison, M. J.,
30 E., Dunlea, J., Huffman, J. A., Onasch, T. B., Alfarra, M. R., Williams, P. I., Bower, K.,
31 Kondo, Y., Schneider, J., Drewnick, F., Borrmann, S., Weimer, S., Demerjian, K., Salcedo,
32 D., Cottrell, L., Griffin, R., Takami, A., Miyoshi, T., Hatakeyama, S., Shimono, A., Sun, J.
33 Y., Zhang, Y. M., Dzepina, K., Kimmel, J. R., Sueper, D., Jayne, J. T., Herndon, S. C.,
34 Trimborn, A. M., Williams, L. R., Wood, E. C., Middlebrook, A. M., Kolb, C. E.,
35 Baltensperger, U. and Worsnop, D. R.: Evolution of Organic Aerosols in the Atmosphere,
36 *Science*, 326(5959), 1525–1529, doi:10.1126/science.1180353, 2009.
- 37 Kameel, F. R., Hoffmann, M. R. and Colussi, A. J.: OH Radical-Initiated Chemistry of
38 Isoprene in Aqueous Media. Atmospheric Implications, *The Journal of Physical Chemistry*
39 *A*, 117(24), 5117–5123, doi:10.1021/jp4026267, 2013.
- 40 Kameel, F. R., Riboni, F., Hoffmann, M. R., Enami, S. and Colussi, A. J.: Fenton Oxidation
41 of Gaseous Isoprene on Aqueous Surfaces, *The Journal of Physical Chemistry C*,
42 140725063829009, doi:10.1021/jp505010e, 2014.
- 43 Kanakidou, M., Seinfeld, J. H., Pandis, S. N., Barnes, I., Dentener, F. J., Facchini, M. C.,
44 Dingenen, R. V., Ervens, B., Nenes, A., Nielsen, C. J. and others: Organic aerosol and
45 global climate modelling: a review, *Atmospheric Chemistry and Physics*, 5(4), 1053–1123,
46 2005.

- 1 Kawamura, K., Kasukabe, H. and Barrie, L. A.: Secondary formation of water-soluble organic
2 acids and α -dicarbonyls and their contributions to total carbon and water-soluble organic
3 carbon: Photochemical aging of organic aerosols in the Arctic spring, *Journal of*
4 *Geophysical Research*, 115(D21), doi:10.1029/2010JD014299, 2010.
- 5 Kroll, J. H., Ng, N. L., Murphy, S. M., Flagan, R. C. and Seinfeld, J. H.: Secondary Organic
6 Aerosol Formation from Isoprene Photooxidation, *Environmental Science & Technology*,
7 40(6), 1869–1877, doi:10.1021/es0524301, 2006.
- 8 Kroll, J. H. and Seinfeld, J. H.: Chemistry of secondary organic aerosol: Formation and
9 evolution of low-volatility organics in the atmosphere, *Atmospheric Environment*, 42(16),
10 3593–3624, doi:10.1016/j.atmosenv.2008.01.003, 2008.
- 11 Kuwata, M., Zorn, S. R. and Martin, S. T.: Using Elemental Ratios to Predict the Density of
12 Organic Material Composed of Carbon, Hydrogen, and Oxygen, *Environmental Science &*
13 *Technology*, 46(2), 787–794, doi:10.1021/es202525q, 2012.
- 14 Lee, A. K. Y., Hayden, K. L., Herckes, P., Leitch, W. R., Liggio, J., Macdonald, A. M. and
15 Abbatt, J. P. D.: Characterization of aerosol and cloud water at a mountain site during
16 WACS 2010: secondary organic aerosol formation through oxidative cloud processing,
17 *Atmospheric Chemistry and Physics*, 12(15), 7103–7116, doi:10.5194/acp-12-7103-2012,
18 2012.
- 19 Lee, A. K. Y., Herckes, P., Leitch, W. R., Macdonald, A. M. and Abbatt, J. P. D.: Aqueous
20 OH oxidation of ambient organic aerosol and cloud water organics: Formation of highly
21 oxidized products: AQUEOUS OXIDATION OF AMBIENT ORGANICS, *Geophysical*
22 *Research Letters*, 38(11), n/a–n/a, doi:10.1029/2011GL047439, 2011a.
- 23 Lee, A. K. Y., Zhao, R., Gao, S. S. and Abbatt, J. P. D.: Aqueous-Phase OH Oxidation of
24 Glyoxal: Application of a Novel Analytical Approach Employing Aerosol Mass
25 Spectrometry and Complementary Off-Line Techniques, *The Journal of Physical*
26 *Chemistry A*, 115(38), 10517–10526, doi:10.1021/jp204099g, 2011b.
- 27 Lee, W., Baasandorj, M., Stevens, P. S. and Hites, R. A.: Monitoring OH-initiated oxidation
28 kinetics of isoprene and its products using online mass spectrometry, *Environmental*
29 *science & technology*, 39(4), 1030–1036, 2005.
- 30 Legrand, M., Preunkert, S., Oliveira, T., Pio, C. A., Hammer, S., Gelencsér, A., Kasper-Giebl,
31 A. and Laj, P.: Origin of C2–C5 dicarboxylic acids in the European atmosphere inferred
32 from year-round aerosol study conducted at a west-east transect, *J. Geophys. Res.*,
33 112(D23), D23S07, doi:10.1029/2006JD008019, 2007.
- 34 Lim, Y. B., Tan, Y. and Turpin, B. J.: Chemical insights, explicit chemistry, and yields of
35 secondary organic aerosol from OH radical oxidation of methylglyoxal and glyoxal in the
36 aqueous phase, *Atmospheric Chemistry and Physics*, 13(17), 8651–8667, doi:10.5194/acp-
37 13-8651-2013, 2013.
- 38 Liu, P. S. K., Deng, R., Smith, K. A., Williams, L. R., Jayne, J. T., Canagaratna, M. R.,
39 Moore, K., Onasch, T. B., Worsnop, D. R. and Deshler, T.: Transmission Efficiency of an
40 Aerodynamic Focusing Lens System: Comparison of Model Calculations and Laboratory
41 Measurements for the Aerodyne Aerosol Mass Spectrometer, *Aerosol Science and*
42 *Technology*, 41(8), 721–733, doi:10.1080/02786820701422278, 2007.
- 43 Liu, Y., Siekmann, F., Renard, P., El Zein, A., Salque, G., El Haddad, I., Temime-Roussel,
44 B., Voisin, D., Thissen, R. and Monod, A.: Oligomer and SOA formation through aqueous

- 1 phase photooxidation of methacrolein and methyl vinyl ketone, *Atmospheric Environment*,
2 49, 123–129, doi:10.1016/j.atmosenv.2011.12.012, 2012.
- 3 Miyakawa, T., Matsuzawa, R., Katayama, M. and Takegawa, N.: Reconsidering Adhesion
4 and Bounce of Submicron Particles Upon High-Velocity Impact, *Aerosol Science and*
5 *Technology*, 47(5), 472–481, doi:10.1080/02786826.2013.763895, 2013.
- 6 Ng, N. L., Canagaratna, M. R., Jimenez, J. L., Chhabra, P. S., Seinfeld, J. H. and Worsnop, D.
7 R.: Changes in organic aerosol composition with aging inferred from aerosol mass spectra,
8 *Atmospheric Chemistry and Physics*, 11(13), 6465–6474, doi:10.5194/acp-11-6465-2011,
9 2011.
- 10 Ng, N. L., Canagaratna, M. R., Zhang, Q., Jimenez, J. L., Tian, J., Ulbrich, I. M., Kroll, J. H.,
11 Docherty, K. S., Chhabra, P. S., Bahreini, R., Murphy, S. M., Seinfeld, J. H., Hildebrandt,
12 L., Donahue, N. M., DeCarlo, P. F., Lanz, V. A., Prévôt, A. S. H., Dinar, E., Rudich, Y.
13 and Worsnop, D. R.: Organic aerosol components observed in Northern Hemispheric
14 datasets from Aerosol Mass Spectrometry, *Atmospheric Chemistry and Physics*, 10(10),
15 4625–4641, doi:10.5194/acp-10-4625-2010, 2010.
- 16 Odian, G. G.: Principles of polymerization, Wiley, Hoboken, N.J. [online] Available from:
17 <http://public.eblib.com/EBLPublic/PublicView.do?ptiID=469767> (Accessed 10 October
18 2014), 2004.
- 19 Ortiz-Montalvo, D. L., Lim, Y. B., Perri, M. J., Seitzinger, S. P. and Turpin, B. J.: Volatility
20 and Yield of Glycolaldehyde SOA Formed through Aqueous Photochemistry and Droplet
21 Evaporation, *Aerosol Science and Technology*, 46(9), 1002–1014,
22 doi:10.1080/02786826.2012.686676, 2012.
- 23 Perri, M. J., Seitzinger, S. and Turpin, B. J.: Secondary organic aerosol production from
24 aqueous photooxidation of glycolaldehyde: Laboratory experiments, *Atmospheric*
25 *Environment*, 43(8), 1487–1497, doi:10.1016/j.atmosenv.2008.11.037, 2009.
- 26 Renard, P., Reed Harris, A. E., Rapf, R. J., Ravier, S., Demelas, C., Coulomb, B., Quivet, E.,
27 Vaida, V. and Monod, A.: Aqueous Phase Oligomerization of Methyl Vinyl Ketone by
28 Atmospheric Radical Reactions, *The Journal of Physical Chemistry C* [online] Available
29 from: <http://pubs.acs.org/doi/abs/10.1021/jp5065598> (Accessed 23 October 2014), 2014.
- 30 Renard, P., Siekmann, F., Gandolfo, A., Socorro, J., Salque, G., Ravier, S., Quivet, E.,
31 Clément, J.-L., Traikia, M., Delort, A.-M., Voisin, D., Vuitton, V., Thissen, R. and Monod,
32 A.: Radical mechanisms of methyl vinyl ketone oligomerization through aqueous phase
33 OH-oxidation: on the paradoxical role of dissolved molecular oxygen, *Atmospheric*
34 *Chemistry and Physics*, 13(13), 6473–6491, doi:10.5194/acp-13-6473-2013, 2013.
- 35 Spracklen, D. V., Jimenez, J. L., Carslaw, K. S., Worsnop, D. R., Evans, M. J., Mann, G. W.,
36 Zhang, Q., Canagaratna, M. R., Allan, J., Coe, H., McFiggans, G., Rap, A. and Forster, P.:
37 Aerosol mass spectrometer constraint on the global secondary organic aerosol budget,
38 *Atmospheric Chemistry and Physics*, 11(23), 12109–12136, doi:10.5194/acp-11-12109-
39 2011, 2011.
- 40 Surratt, J. D., Murphy, S. M., Kroll, J. H., Ng, N. L., Hildebrandt, L., Sorooshian, A.,
41 Szmigielski, R., Vermeylen, R., Maenhaut, W., Claeys, M., Flagan, R. C. and Seinfeld, J.
42 H.: Chemical Composition of Secondary Organic Aerosol Formed from the Photooxidation
43 of Isoprene, *The Journal of Physical Chemistry A*, 110(31), 9665–9690,
44 doi:10.1021/jp061734m, 2006.

- 1 Tan, Y., Carlton, A. G., Seitzinger, S. P. and Turpin, B. J.: SOA from methylglyoxal in clouds
2 and wet aerosols: Measurement and prediction of key products, *Atmospheric Environment*,
3 44(39), 5218–5226, doi:10.1016/j.atmosenv.2010.08.045, 2010.
- 4 Tan, Y., Lim, Y. B., Altieri, K. E., Seitzinger, S. P. and Turpin, B. J.: Mechanisms leading to
5 oligomers and SOA through aqueous photooxidation: insights from OH radical oxidation
6 of acetic acid and methylglyoxal, *Atmospheric Chemistry and Physics*, 12(2), 801–813,
7 doi:10.5194/acp-12-801-2012, 2012.
- 8 Tan, Y., Perri, M. J., Seitzinger, S. P. and Turpin, B. J.: Effects of Precursor Concentration
9 and Acidic Sulfate in Aqueous Glyoxal–OH Radical Oxidation and Implications for
10 Secondary Organic Aerosol, *Environmental Science & Technology*, 43(21), 8105–8112,
11 doi:10.1021/es901742f, 2009.
- 12 Volkamer, R., San Martini, F., Molina, L. T., Salcedo, D., Jimenez, J. L. and Molina, M. J.: A
13 missing sink for gas-phase glyoxal in Mexico City: Formation of secondary organic
14 aerosol, *Geophysical Research Letters*, 34(19), doi:10.1029/2007GL030752, 2007.
- 15 Zhang, X., Chen, Z. M. and Zhao, Y.: Laboratory simulation for the aqueous OH-oxidation of
16 methyl vinyl ketone and methacrolein: significance to the in-cloud SOA production,
17 *Atmospheric Chemistry and Physics*, 10(19), 9551–9561, doi:10.5194/acp-10-9551-2010,
18 2010.
- 19 Zhao, R., Lee, A. K. Y. and Abbatt, J. P. D.: Investigation of Aqueous-Phase Photooxidation
20 of Glyoxal and Methylglyoxal by Aerosol Chemical Ionization Mass Spectrometry:
21 Observation of Hydroxyhydroperoxide Formation, *The Journal of Physical Chemistry A*,
22 116(24), 6253–6263, doi:10.1021/jp211528d, 2012.

Exp. Name	[MVK] ₀ (mM)	[H ₂ O ₂] ₀ (mM)	MVK 90% Consumption time (min)
A	20	400	120
B	5	100	50
C	2	40	30
D	0.5	10	25
E	0.2	4	20

Table 1: Experimental conditions of $\cdot\text{OH}$ -oxidation of MVK in the aqueous phase. All experiments are performed at 25°C. Time 0 corresponds to MVK injection in the photoreactor (samples taken at 0, 5, 10, 15, 30, 50, 75, 105, 150 min). Aqueous phase characterization was performed using UPLC-ESI-MS and UHPLC-UV for all experiments, and IC-ESI-MS analyses were made only during experiments A and B. Aerosol characterization after nebulization using SMPS and AMS was performed for all experiments.

Reaction Time (min)	D_p (nm) ^a	N ($\times 10^3 \text{ cm}^{-3}$) ^a	H/C ^b	O/C ^b	ρ_{org} (g cm^{-3}) ^{b,c}	M_{SMPS} ($\mu\text{g m}^{-3}$) ^{a,d}	Yield (%) ^{a,d,e}
5	28.3 ± 0.7	90 ± 6	1.55 ± 0.02	0.28 ± 0.05	1.0 ± 0.2	10 ± 10	70 ± 80
15	38 ± 1	530 ± 30	1.55 ± 0.01	0.26 ± 0.01	1.1 ± 0.1	100 ± 20	90 ± 60
50	44 ± 1	860 ± 40	1.55 ± 0.01	0.29 ± 0.01	1.1 ± 0.1	240 ± 50	80 ± 50
105	37 ± 1	1200 ± 50	1.47 ± 0.01	0.42 ± 0.01	1.2 ± 0.2	220 ± 40	70 ± 40
150	35 ± 1	1310 ± 50	1.38 ± 0.01	0.57 ± 0.01	1.4 ± 0.2	200 ± 30	60 ± 40

Table 2: Characteristics of the aerosol formed from nebulized MVK-solutions at different reaction times for experiment B.

Values are the average of ^a three consecutive SMPS measurements, and ^b five consecutive O/C and H/C AMS measurements, and uncertainties represent the corresponding standard deviation of these averages.

^c Particle densities are calculated using the method by Kuwata et al. (2012), the associated uncertainties include the accuracy of $\pm 12\%$ stated by these authors for eq.1.

^d Mass concentration values include the corresponding aerosol densities.

^e Yield values and associated uncertainties include dilution + transmission efficiency determined for the nebulizing system (see supplementary information 1).

Exp. Name	[MVK] ₀ (mM)	t _{max} (min) ^a	ρ _{org} (g cm ⁻³) ^b	M _{SMPS} (μg m ⁻³) ^b	Yield (%) ^{b,c}	H/C ^b	O/C ^b
A	20	105	1.1 ± 0.1	900 ± 200	70 ± 50	1.54 ± 0.01	0.30 ± 0.01
B	5	50	1.1 ± 0.1	240 ± 50	80 ± 50	1.55 ± 0.01	0.29 ± 0.01
C	2	30	1.1 ± 0.1	100 ± 20	80 ± 60	1.55 ± 0.01	0.28 ± 0.01

Table 3: Overview of aerosol properties and mass yields for different initial MVK concentrations.

^a Values are given at t_{max}, corresponding to the maximum aerosol mass concentration.

^b All values and associated uncertainties are calculated as indicated in Table 2.

^c Including dilution + transmission efficiency (TE) in the nebulizing system; TE: 17.2 (±7.9) for [MVK]₀ = 2 - 20mM determined from NH₄NO₃ (see supplementary information 1).

1 Figure 1: Schematic overview of the aerosol generation setup.

2

3 Figure 2: (a): Time profiles of MVK concentrations during the reaction (experiment B); and
4 the corresponding evolution of ESI-MS- spectra for m/z 50 - 1200 at (b): 5 min, (c): 50 min
5 and (d): 150 min. Highlighted in red in (c), the most intense peaks of the main series of
6 oligomers together with its related molecular structure.

7

8 Figure 3: Time profiles of the HR-ToF-AMS total organic mass (red), ion fragments
9 $C_2H_3O^+$ at m/z 43 (blue) and CO_2^+ m/z 44 (green) for nebulized solutions from experiment
10 B (a), and the corresponding evolution of HR-ToF-AMS mass spectra (for m/z 0 - 100) for
11 nebulized solutions sampled after 5 min (b), 50 min (c) and 150 min (d). Values are averages
12 of 5 consecutive HR-ToF-AMS-runs, error bars represent their standard deviations. The
13 AMS-mass fraction is the signal intensity contribution of each fragment to the total signal.

14

15 Figure 4: Comparison of HR-ToF-AMS mass spectra (in the range 100 - 200 amu) of the
16 nebulized solutions sampled from experiment B after 50 and 150 min of reaction in the
17 aqueous phase. The AMS-mass fraction is the signal intensity contribution of each fragment
18 to the total signal.

19

20 Figure 5: Evolution of particle number (a) and mass (b) size distributions for nebulized
21 solutions sampled at different reaction times for experiment B, measured by means of SMPS.
22 The standard deviations are smaller than the width of the symbols

23

24 Figure 6: Time profiles of the total aerosol mass (black diamonds) from the nebulized
25 solutions, and consumed MVK in the aqueous phase (red circles) for experiment B. a Values
26 represent averages of three consecutive SMPS-measurements for each reaction time
27 considering the corresponding density (Table 1). Error bars represent the sum of the standard
28 deviation of these averages and the uncertainties of the density calculation. b % in
29 concentration of MVK. These concentrations were determined by means of UHPLC-UV, with
30 an uncertainty of ± 2 %.

31

32 Figure 7: Influence of the initial MVK concentration on the evolution of the total SOA mass
33 obtained from the nebulized solutions. Values represent averages of three consecutive SMPS-

1 measurements for each reaction time considering the corresponding density (Table 3). Error
2 bars represent the standard deviation of these averages and the uncertainties of the density
3 calculation. For the lowest initial concentrations (experiments D and E), blank signals were
4 subtracted, and a density of 1.1 g cm^{-3} was assumed.

5
6 Figure 8: Fractions f_{44} versus f_{43} for the nebulized solutions from experiments A, B, C, D
7 and E, as measured by the HR-ToF-AMS are compared to ambient air LV-OOA and SV-
8 OOA from the compilation by Ng et al. (2010) (dashed black triangle), and are also compared
9 to the nebulization data by Lee et al. (2011a) (dotted grey triangle). For our experiments, the
10 signal from blank experiments was subtracted. The data are shown for experiments A, B, and
11 C from 10 to 150 min of reaction, and for experiments D and E from 15 to 150 min of
12 reaction. The gas/particle partitioning in our set up may alter the relative oxygenation of the
13 OA produced, especially at low initial concentrations.

14
15 Figure 9: Van Krevelen diagram for the nebulized solutions of experiment C, as measured by
16 the AMS. Only experiment C is shown for clarity as the data for experiments A and B are
17 stacked together with the data shown. a Red diamonds represent the elemental ratios of
18 oligomers with a Degree of Polymerization = 5 for the ten most abundant oligomer series
19 identified by Renard et al. (2013). The black dotted circle highlights compounds with similar
20 structures. b Ng et al., 2011, for details see text section 4.2.

21
22 Figure 10 : Time profiles of the quantified diacids in the solutions as measured by IC-ESI-MS
23 for experiment B ($[\text{MVK}]_0 = 5 \text{ mM}$).

24
25 Figure 11: Potential atmospheric fate of MVK in the aqueous phase. X-Axis denotes volatility
26 (\log_{10} of C^* at 298K), y-axis denotes oxidation state, approximated by O/C (Jimenez et al.,
27 2009).

1
2
3
4

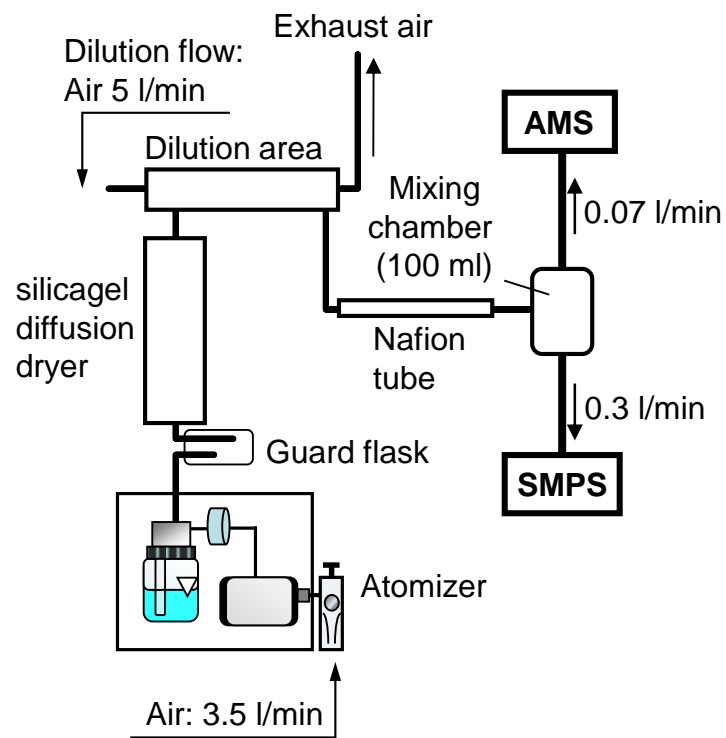


Figure 1: Schematic overview of the aerosol generation setup.

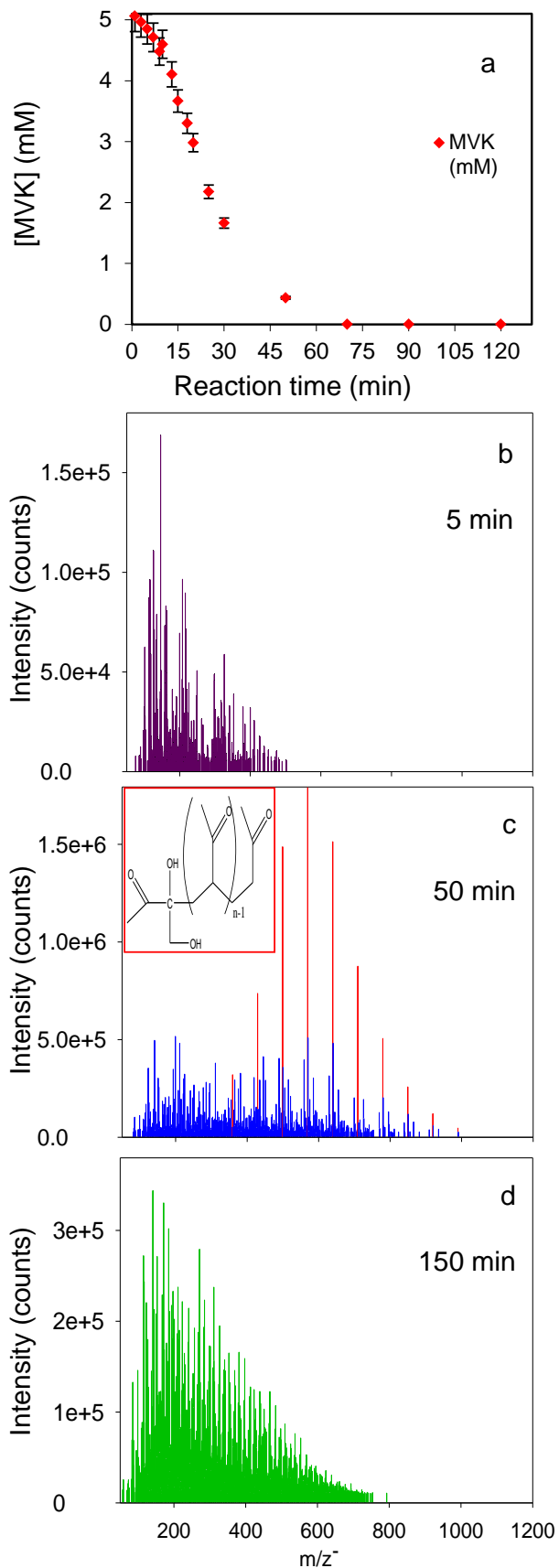
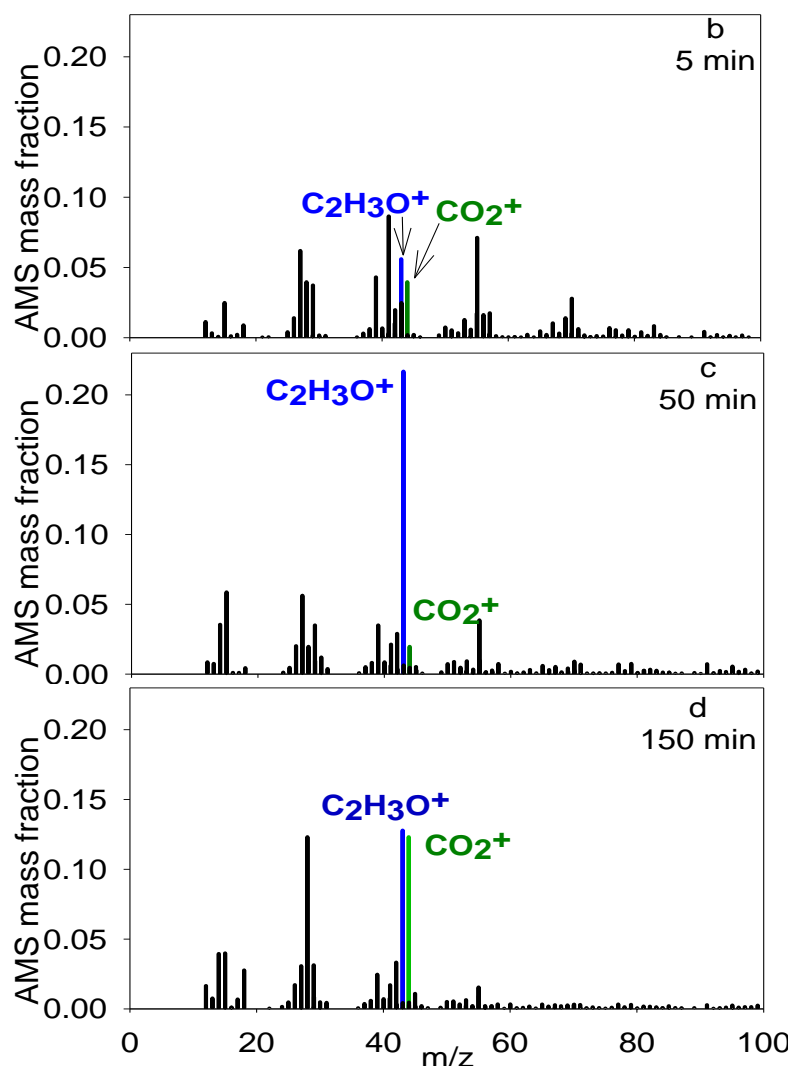
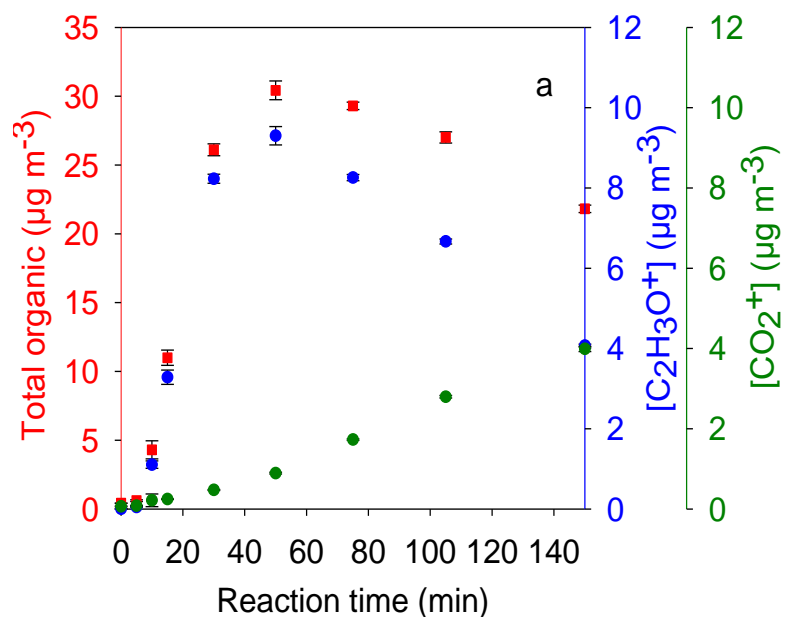


Figure 2: (a): Time profiles of MVK concentrations during the reaction (experiment B); and the corresponding evolution of ESI-MS spectra for m/z 50 - 1200 at (b): 5 min, (c): 50 min and (d): 150 min. Highlighted in red in (c), the most intense peaks of the main series of oligomers together with its related molecular structure.

1
2

Figure 3: Time profiles of the HR-ToF-AMS total organic mass (red), ion fragments $C_2H_3O^+$ at m/z 43 (blue) and CO_2^+ m/z 44 (green) for nebulized solutions from experiment B (a), and the corresponding evolution of HR-ToF-AMS mass spectra (for m/z 0 - 100) for nebulized solutions sampled after 5 min (b), 50 min (c) and 150 min (d). Values are averages of 5 consecutive HR-ToF-AMS-runs, error bars represent their standard deviations. The AMS-mass fraction is the signal intensity contribution of each fragment to the total signal.



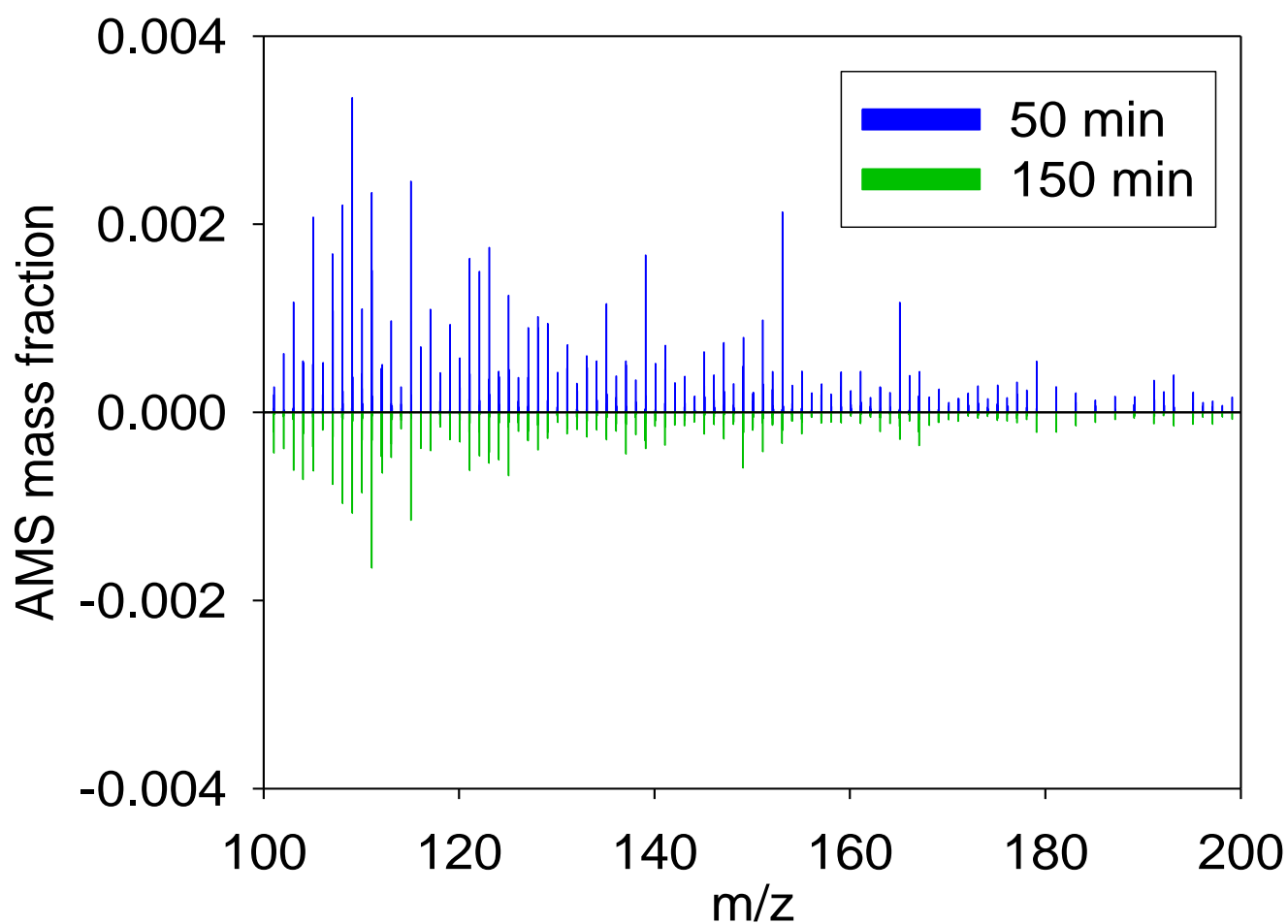


Figure 4: Comparison of HR-ToF-AMS mass spectra (in the range 100 - 200 amu) of the nebulized solutions sampled from experiment B after 50 and 150 min of reaction in the aqueous phase. The AMS-mass fraction is the signal intensity contribution of each fragment to the total signal.

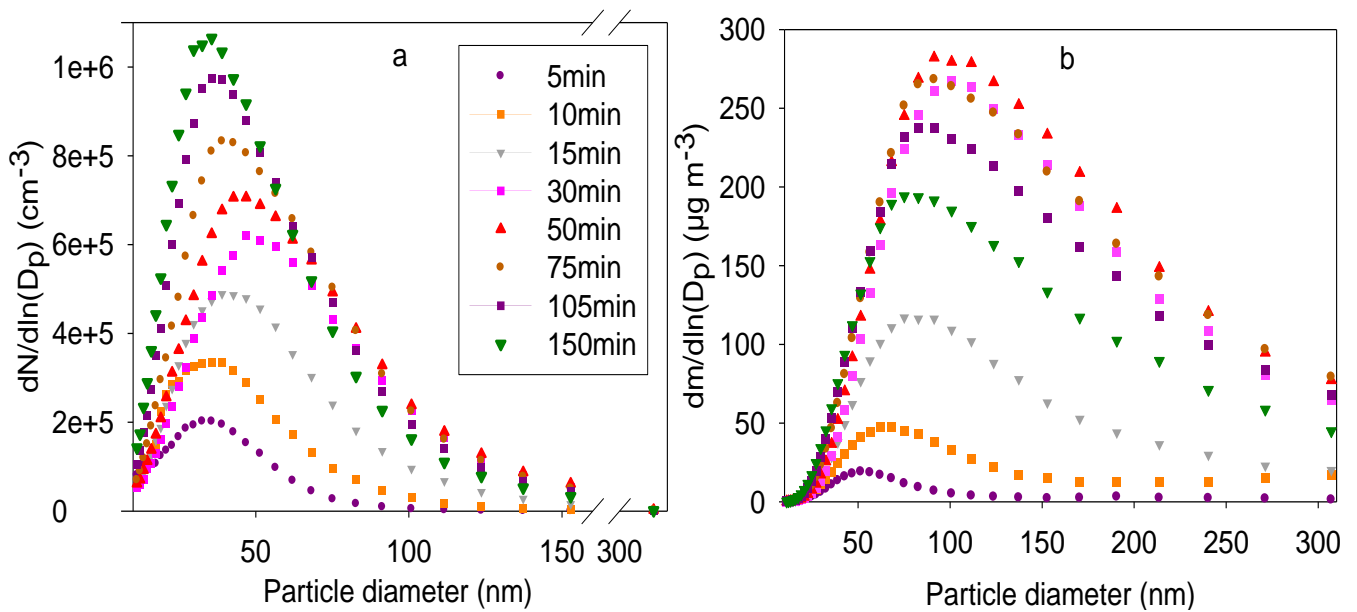


Figure 5: Evolution of particle number (a) and mass (b) size distributions for nebulized solutions sampled at different reaction times for experiment B, measured by means of SMPS. The standard deviations are smaller than the width of the symbols

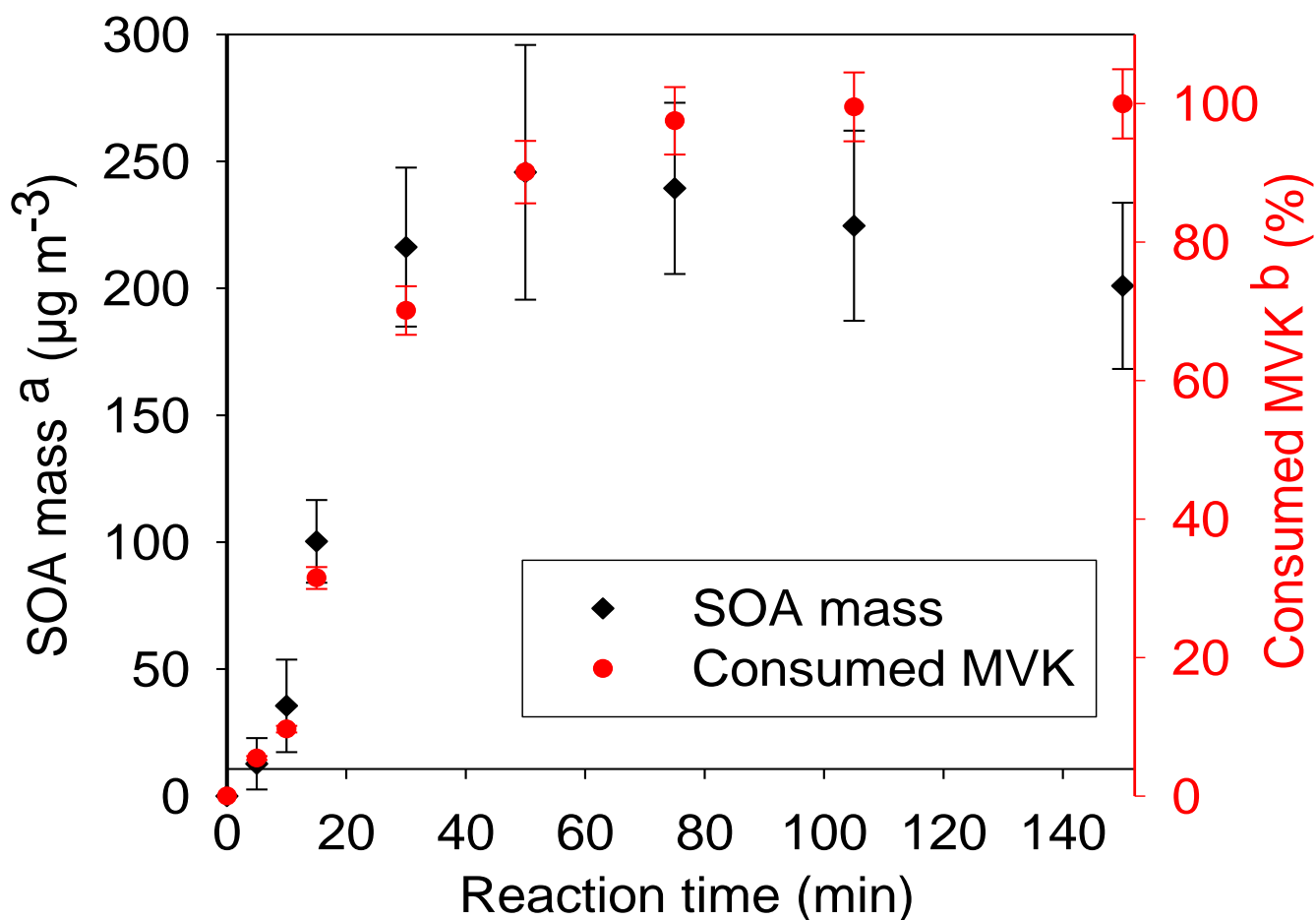


Figure 6: Time profiles of the total aerosol mass (black diamonds) from the nebulized solutions, and consumed MVK in the aqueous phase (red circles) for experiment B. ^a Values represent averages of three consecutive SMPS-measurements for each reaction time considering the corresponding density (Table 1). Error bars represent the sum of the standard deviation of these averages and the uncertainties of the density calculation. ^b % in concentration of MVK. These concentrations were determined by means of UHPLC-UV, with an uncertainty of ± 2 %.

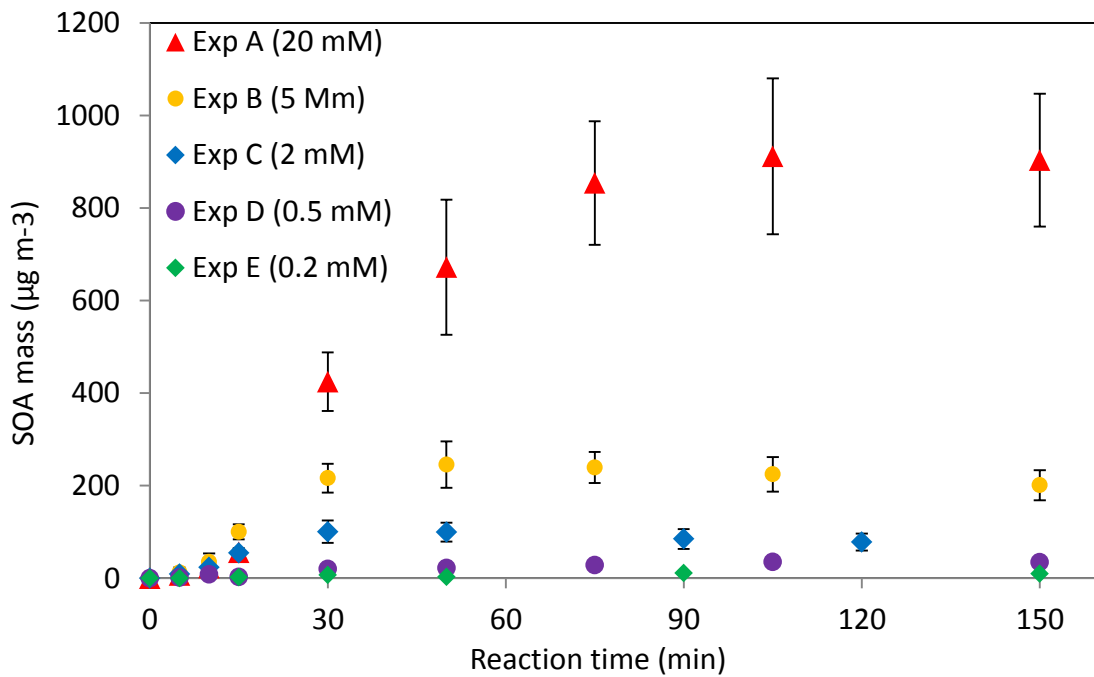


Figure 7: Influence of the initial MVK concentration on the evolution of the total SOA mass obtained from the nebulized solutions. Values represent averages of three consecutive SMPS-measurements for each reaction time considering the corresponding density (Table 3). Error bars represent the standard deviation of these averages and the uncertainties of the density calculation. For the lowest initial concentrations (experiments D and E), blank signals were subtracted, and a density of 1.1 g cm^{-3} was assumed.

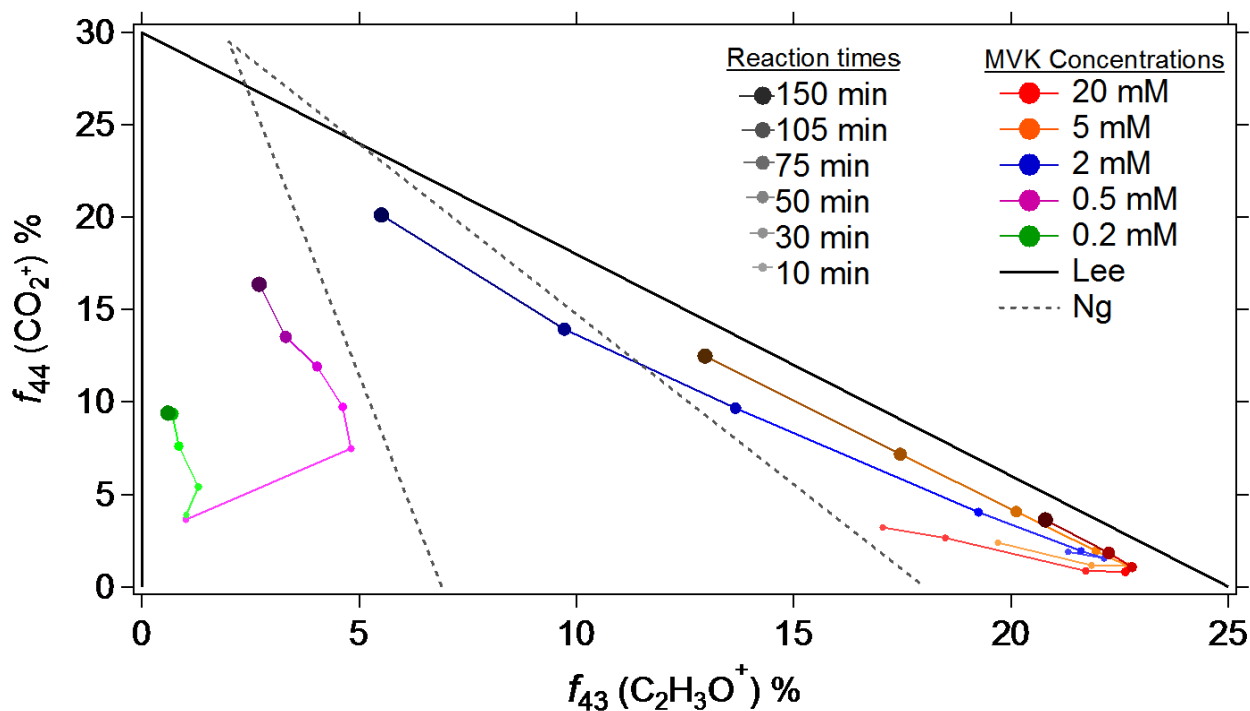


Figure 8: Fractions f_{44} versus f_{43} for the nebulized solutions from experiments A, B, C, D and E, as measured by the HR-ToF-AMS are compared to ambient air LV-OOA and SV-OOA from the compilation by Ng et al. (2010) (dashed black triangle), and are also compared to the nebulization data by Lee et al. (2011a) (dotted grey triangle). For our experiments, the signal from blank experiments was subtracted. The data are shown for experiments A, B, and C from 10 to 150 min of reaction, and for experiments D and E from 15 to 150 min of reaction. The gas/particle partitioning in our set up may alter the relative oxygenation of the OA produced, especially at low initial concentrations.

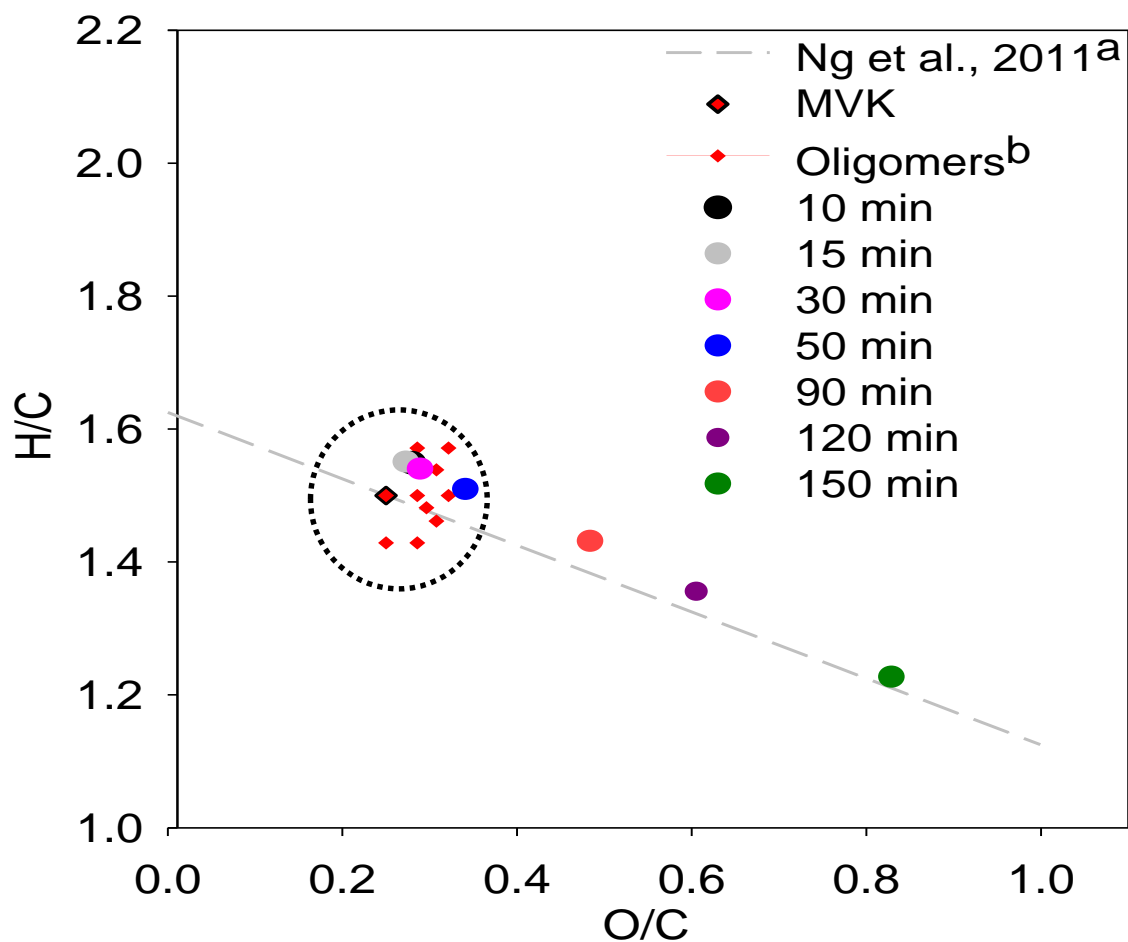


Figure 9: Van Krevelen diagram for the nebulized solutions of experiment C, as measured by the AMS. Only experiment C is shown for clarity as the data for experiments A and B are stacked together with the data shown. ^a Red diamonds represent the elemental ratios of oligomers with a Degree of Polymerization = 5 for the ten most abundant oligomer series identified by Renard et al. (2013). The black dotted circle highlights compounds with similar structures. ^b Ng et al., 2011, for details see text section 4.2.

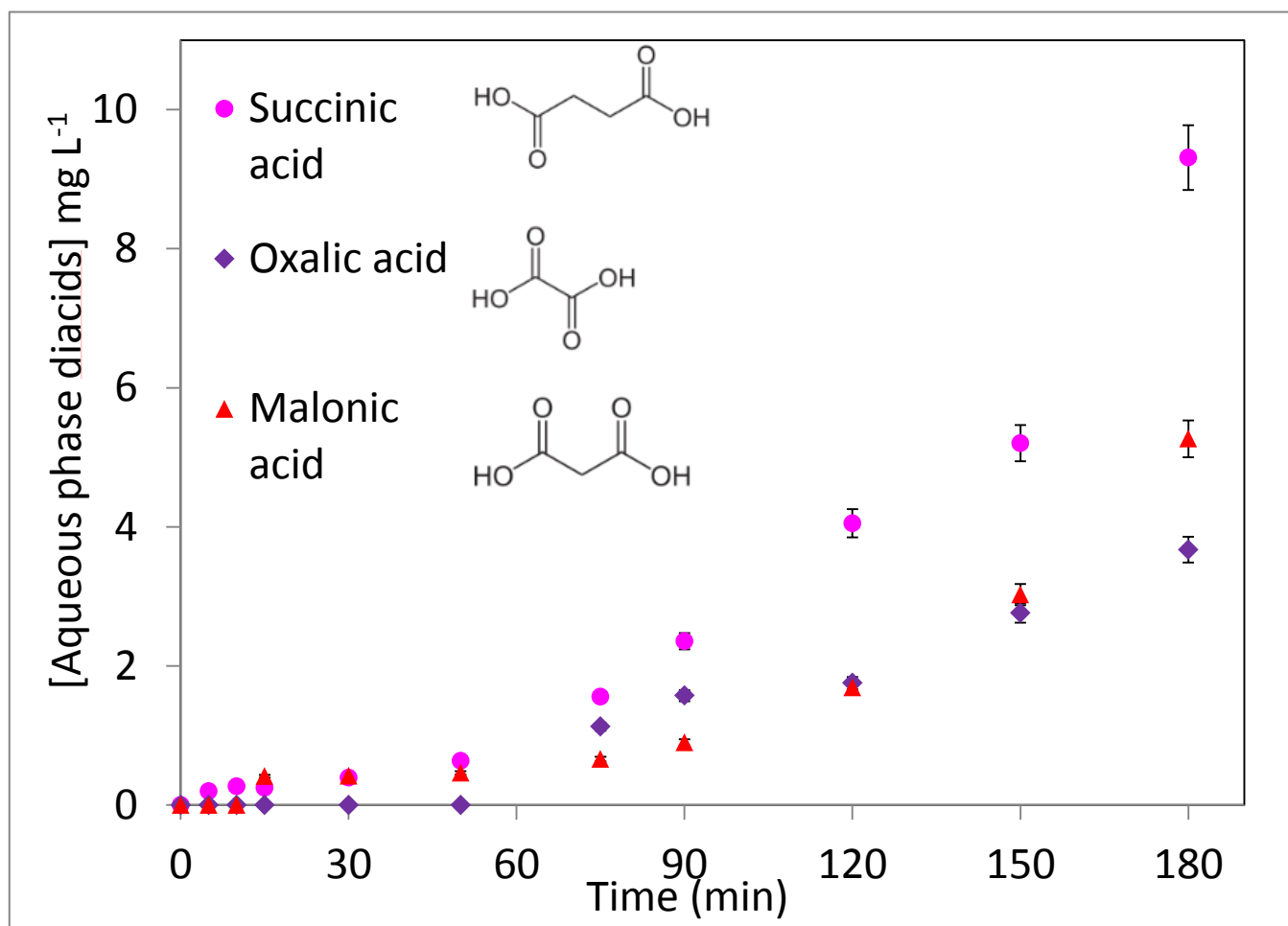


Figure 10 : Time profiles of the quantified diacids in the solutions as measured by IC-ESI-MS for experiment B ([MVK]₀ = 5 mM).

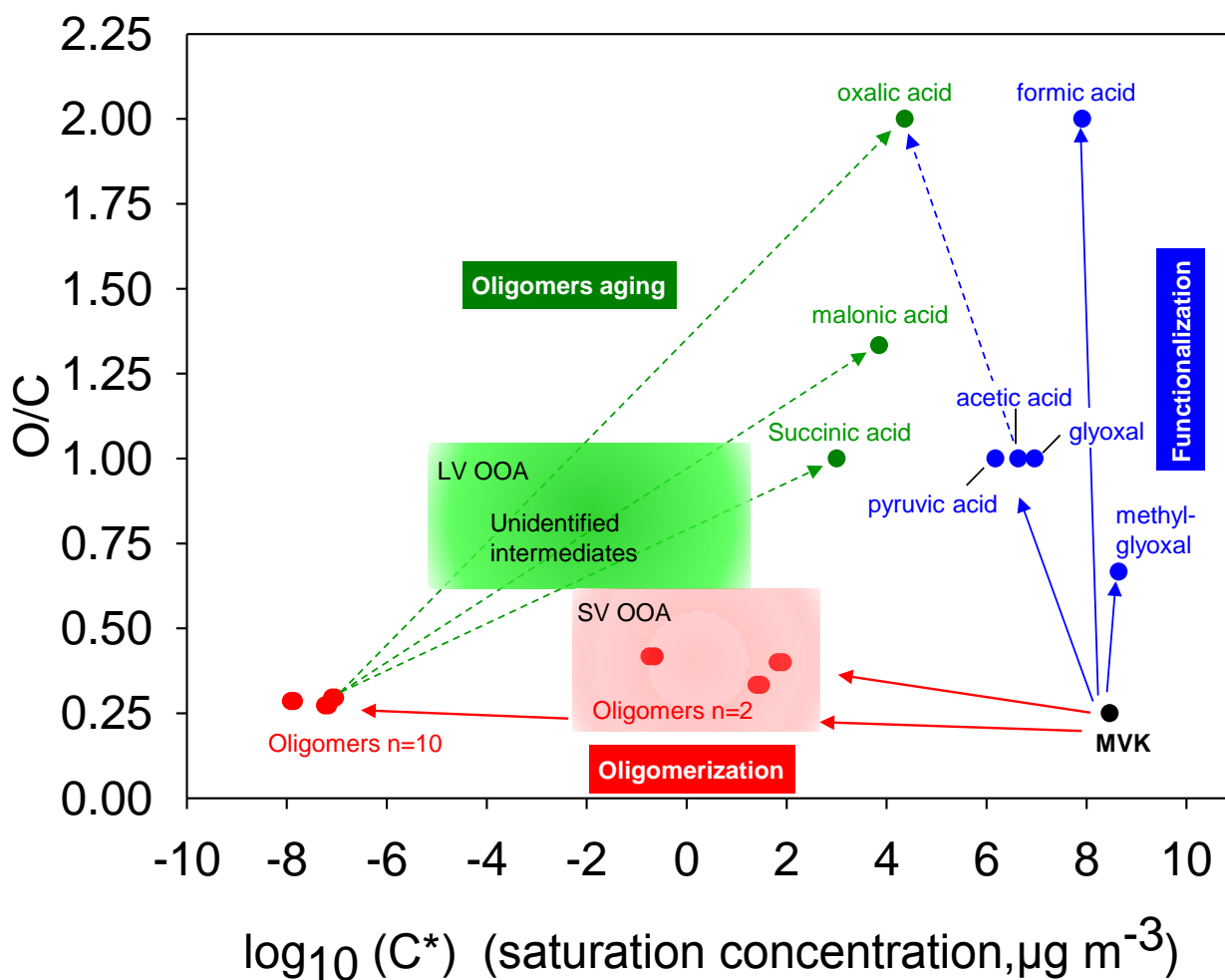


Figure 11: Potential atmospheric fate of MVK in the aqueous phase. X-Axis denotes volatility (\log_{10} of C^* at 298K), y-axis denotes oxidation state, approximated by O/C (Jimenez et al., 2009).

Supplementary Information

Supplementary Information 1: Calibration experiments of our set up

Calibration experiments of our set up were performed using aqueous solutions of three different compounds (NaCl, NH₄NO₃, and succinic acid) at various concentrations covering those of the consumed MVK during its reaction (Table S1). In these calibration experiments, for each compound, the obtained numbers of particles increase with increasing solution concentrations, and the corresponding total particle mass (using the corresponding densities) increases linearly with the solution concentration. This result was used to evaluate the transmission efficiency of our set up. Assuming a similar behavior for the nebulized MVK-oligomers up to t_{max} (i.e. increasing oligomer concentrations with reaction time, assuming no major change in the oligomer composition), the calibration experiments were used to determine the SOA mass yields according to equations 2 and 3. The differences obtained between the three calibration experiments may be due to the different physical properties of the particles (e.g. volatility, surface tension and hygroscopicity) linked to their chemical composition. Table S1 shows that the solutions of NaCl generated a significantly higher transmission efficiency than the solutions of NH₄NO₃ and succinic acid. It is likely that the properties of the SOA generated from the nebulized solutions of oxidized MVK were closer to that of NH₄NO₃ and succinic acid than NaCl. Finally, the transmission efficiency obtained for NH₄NO₃ solutions was used to calculate the SOA mass yields according to equations 2 and 3.

Compound	Range of aqueous phase concentration (mg L ⁻¹)	Range of particle mass concentration after nebulization (μg m ⁻³)	Particle density (g cm ⁻³)	Transmission efficiency (%)
Succinic acid	50 - 2000	20 - 1300	1.56	13.1 (± 2.6)
NH ₄ NO ₃	30 - 3000	10 - 4500	1.73	17.2 (± 7.9)
NaCl	50 - 2000	100 - 4000	2.17	44.6 (± 2.3)

Table S1: Determination of particle transmission efficiency in the particle generation system

Supplementary Information 2: Average spectral irradiance of the Xe lamps

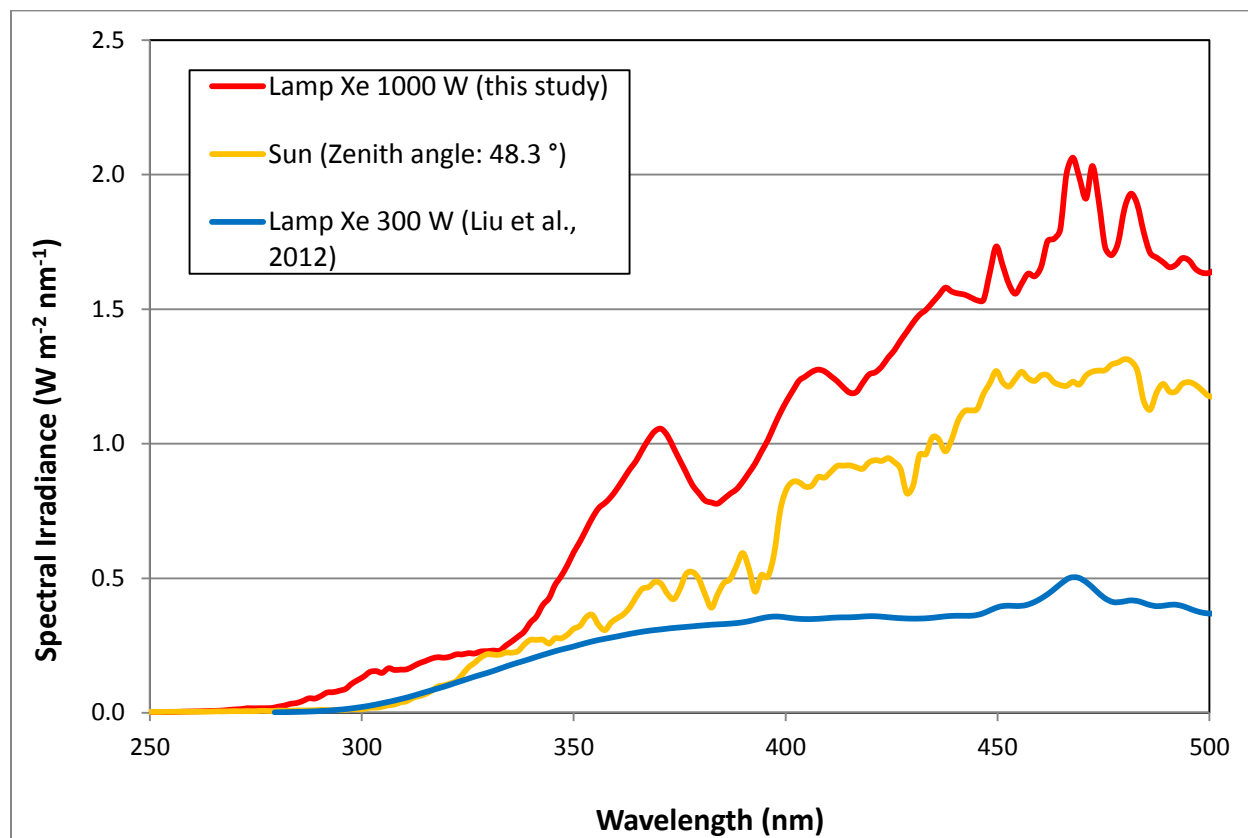


Figure S1: Figure S1: Average spectral irradiance of the Xe lamps 1000 W with a ASTM 490 AM 0 filter (in red, used in the present study), 300 W with a pyrex filter (in blue, Liu et al., 2012), and as compared to the direct solar irradiance at sea level, for a 48.3° zenith angle (in orange).

Supplementary Information 3: Determination of $\cdot\text{OH}$ concentrations in the solution

$\cdot\text{OH}$ concentrations were calculated by means of two different methods (methods a) and b) below), which gave similar results:

a) Considering reactions R1 to R3, $\cdot\text{OH}$ concentrations were calculated assuming the steady state approximation at time 0:

$$[\text{OH}] = \frac{2 \times J_{\text{H}_2\text{O}_2} \times [\text{H}_2\text{O}_2]}{k_3 \times [\text{MVK}] + k_2 \times [\text{H}_2\text{O}_2]}$$



$J_{\text{H}_2\text{O}_2}$ was determined by fitting H_2O_2 concentration decay



$$k_2 = 2.95 \cdot 10^7 \text{ M}^{-1} \text{ s}^{-1} \text{ at } 25^\circ \text{C} \quad (\text{Christensen et al., 1982})$$



$$k_3 = 7.3.(\pm 0,5) 10^9 \text{ M}^{-1} \text{ s}^{-1} \text{ at } 25^\circ \text{C} \quad (\text{Schöne et al., 2014})$$

The obtained values are $[\cdot\text{OH}] = (6 - 5) \times 10^{-14} \text{ M}$ (for pH 6 – 3 respectively)

b) Fitting the initial MVK decay with an exponential decay:

$$[\text{MVK}]_t = [\text{MVK}]_0 \times e^{-(k_3 \times [\cdot\text{OH}] \times t)}$$

With $k_3 = 7,3.(\pm 0,5) 10^9 \text{ M}^{-1} \text{ s}^{-1}$ at 25°C (Schöne et al., 2014), we obtained similar values for $\cdot\text{OH}$ steady state concentrations ($[\cdot\text{OH}] = 2 \times 10^{-14} \text{ M}$) as for method a).

References Supplementary Information

- Christensen, H., Sehested, K. and Corfitzen, H.: Reactions of hydroxyl radicals with hydrogen peroxide at ambient and elevated temperatures, *J. Phys. Chem.*, 86(9), 1588–1590, doi:10.1021/j100206a023, 1982.
- Liu, Y., Siekmann, F., Renard, P., El Zein, A., Salque, G., El Haddad, I., Temime-Roussel, B., Voisin, D., Thissen, R. and Monod, A.: Oligomer and SOA formation through aqueous phase photooxidation of methacrolein and methyl vinyl ketone, *Atmospheric Environment*, 49, 123–129, doi:10.1016/j.atmosenv.2011.12.012, 2012.
- Schöne, L., Schindelka, J., Szeremeta, E., Schaefer, T., Hoffmann, D., Rudzinski, K. J., Szmigielski, R. and Herrmann, H.: Atmospheric aqueous phase radical chemistry of the isoprene oxidation products methacrolein, methyl vinyl ketone, methacrylic acid and acrylic acid – kinetics and product studies, *Physical Chemistry Chemical Physics*, 16(13), 6257, doi:10.1039/c3cp54859g, 2014.